Ore Geology Reviews 74 (2016) 170–195

Contents lists available at ScienceDirect

Ore Geology Reviews

journal homepage: www.elsevier.com/locate/oregeorev

# Structural evolution of the Mokrsko-West, Mokrsko-East and Čelina gold deposits, Bohemian Massif, Czech Republic: Role of fluid overpressure

Jiří Zachariáš

*Institute of Geochemistry, Mineralogy and Mineral Resources, Faculty of Science, Charles University in Prague, Albertov 6, 128 43 Prague 2, Czech Republic*

ARTICLE INFO

*Article history:*
Received 2 April 2015
Received in revised form 16 November 2015
Accepted 20 November 2015
Available online 22 November 2015

*Keywords:*
Gold deposits;
Vein thickness;
Vein spacing;
Fluid pressure;
Paleostress;
Bohemian Massif

ABSTRACT

The studied Mokrsko-West (90–100 t Au), Mokrsko-East (30 t Au) and Čelina (11 t Au) deposits represent three spatially and genetically interrelated deposits of supposed affiliation to the intrusion-related gold deposit type. The deposits differ in their dominant host rocks, which are represented by ca 354 Ma old biotite tonalite (Mokrsko-West) and Neoproterozoic volcanic and volcanosedimentary rocks (Mokrsko-East, Čelina). Another difference lies in the style of veining — densely spaced networks of 0.1–5 mm thin veins ($Q_2$) within the tonalite, compared to thick (usually 5–20 cm; $Q_{1-2}$) and widely spaced veins within the Neoproterozoic rocks.

Five generations of quartz veins, referred to as $Q_0$ through $Q_4$ were distinguished: $Q_0$ veins are the oldest and ore-barren, $Q_1$ veins mark the onset of the Au-ore formation, $Q_2$ veins its culmination and $Q_3$ veins its fading. Late quartz gangue ($Q_4$) is associated with uneconomic Ag–Pb–Zn vein-type ores hosted by calcite–barite–(quartz) veins.

Quartz vein thickness (~0.3 to ~300 mm), spacing (~3 mm to ~500 mm), distribution, and related extensional strain (ca. 3–25%) evolve systematically across the studied ore district, reflecting both the major host rock and other tectonic factors. Detailed study of vein dimension parameters (thickness, length, width, aspect ratios) allowed estimation of the probable depth of the fluid source reservoir (~2 km or ~4 km) below the present surface. The depth to the fluid source seems to increase through time, being the shallowest for the $Q_0$ veins and the deepest for the $Q_2$ veins. Two independent methods of estimating fluid overpressure are discussed in the paper. Fluid overpressure during vein formation decreases from the $Q_0$ through the $Q_2$ veins, from 10 to 4 MPa or from 26 to 10 MPa, depending on the assumed tensile strength of the tonalite (5.5 and 15 MPa, respectively).

The origin of joints and veins is discussed in terms of the stress orientation and crack-seal and crack-jump mechanisms. Field relationships unambiguously indicate that the veins hosted by Neoproterozoic rocks originated by reopening of the pre-existing extension joints ($J_1$) due to fluid overpressure. The origin of the densely-spaced thin veins ($Q_2$) hosted by the tonalite at the Mokrsko-West deposit is, however, less certain. It is probable that the tonalite was already affected by microfracturing analogous to the $J_1$ joints prior to the formation of quartz veins. The formation of the $Q_{1-2}$ veins at the Mokrsko-East deposit was constrained by the Re–Os dating of molybdenite to 342.9 ± 1.4 Ma. The ore-bearing hydrothermal system is thus ca 12 Ma younger than the tonalite that hosts the Mokrsko-West deposit. A similar ca 15–2 Ma difference between the age of the host-intrusion and the age of the hydrothermal event was encountered in several other gold deposits in the vicinity of the Central Bohemian Plutonic Complex. Two hypotheses to explain this are discussed in the paper.



## 1. Introduction

The Bohemian Massif hosts numerous ore deposits (Au, Ag–Pb–Zn, Sn–W, U) related to Variscan (Hercynian) metallogenic events. Among them, the gold deposits have a remarkable potential for future mining; about 200–300 t of gold is available in the present resources. One-half of them correspond to orogenic gold (Strnad et al., 2012) and the other to intrusion-related gold deposits (Morávek, 1996a; Zachariáš et al., 2014, 2001). Gold deposits in the central part of the Bohemian Massif mostly occur within an approx. 100 km long and 30 km wide zone along the NW-margin of the ~354–335 Ma old Central Bohemian Plutonic Complex (CBPC). The CBPC intruded along the boundary between the low-grade Teplá-Barrandian and the high-grade Moldanubian blocks/units. A common feature of all gold deposits in this zone is their variable but generally low sulfide content (<5 vol.% of pyrite, arsenopyrite and pyrrhotite), high fineness of the gold (usually >90 at.% Au), the presence of Bi–Te–(S)–(Se) phases, scheelite and molybdenite. Formation of these gold deposits occurred from 345 to 338 Ma, thus being in general coeval with the intrusive activity of the CBPC (ca. 354–335 Ma). In detail, however, the individual deposits are an average of about 5 Ma younger than their intrusive-host. For more details on gold metallogeny in the Bohemian Massif and individual case studies, see recent papers (Boiron et al., 2001; Morávek, 1996a; Strnad et al., 2012; Zachariáš et al., 2014, 2013, 2009, 2001).

*E-mail address:* jiri.zacharias@natur.cuni.cz.

http://dx.doi.org/10.1016/j.oregeorev.2015.11.027
0169-1368/

Intrusion-related gold deposits (e.g. Baker, 2002; Duuring et al., 2007; Thompson et al., 1999) represent a relatively new class of gold deposits which are, however, heterogeneous in detail. They often form "sheeted veins", a system of parallel (stacked) quartz veins, usually 1–20 cm wide, moderately to widely spaced (~20 cm to ~2 m) and of variable spatial extent (e.g. Gumiel et al., 2008; Kontak and Kyser, 2011; Otto et al., 2009). Spectacular examples of sheeted veins are also known from another class of granite-related deposits, from Sn–W greisens (e.g. Foxford et al., 2000; Jackson et al., 1989; Sanderson et al., 2008). Similar forms, however of more restricted spatial extent, were also identified at epithermal and porphyry deposits (e.g. Penczak and Mason, 1997).

The studied Mokrsko-West gold deposit represents an outstanding world-class example of a sheeted vein complex. It is composed of densely spaced thin veins (0.1–5 mm thick, up to 200 veins/m) and of widely spaced thicker veins (5–20 cm, 0.2–3 veins/m). Two other spatially-related gold deposits, the Mokrsko-East and Čelina deposits, host only the widely spaced thicker veins. The total gold resources of this gold district approach ~140 t, of which 90–100 t Au represents the Mokrsko-West deposit, 30 t Au the Mokrsko-East deposit and 11 t Au the Čelina deposit (Morávek et al., 1990, 1991b; Morávek, 1996b).

This paper is focused on the structural aspects of the formation of the Mokrsko-West, Mokrsko-East and Čelina deposits. It aims: 1) to elucidate the factors critical for the origin of the densely-spaced sheeted veins; 2) to decipher the role of fluid overpressure in the formation of veins and joints; and 3) to discuss the nature of the about 10 Ma age-difference between the intrusion of the tonalite host and the formation of gold-bearing quartz veins (such an age difference seems quite common in mid—/deep-crustal plutonic settings).

To achieve these goals, detailed structural data from underground and surface exposures of these gold deposits are summarized, complemented by a similar structural study of a much wider area where no gold mineralization is present. Then various approaches are used for unraveling the paleostress history, as well as for quantification of the fluid overpressure and paleostress magnitudes during vein formation. Finally, the depth of the fluid source region is estimated. In the conclusion, a geological model of hydrothermal processes in deep plutonic settings is formulated.

## 2. Geological setting

### 2.1. Regional geology

The Bohemian Massif (BM) represents the easternmost segment of the European Variscan Belt. Traditionally, is divided into four major tectonic units: the Saxothuringian, the Teplá-Barrandian, the Moldanubian and the Moravo-Silesian units (Fig. 1a). Recent models of Variscan geotectonic evolution of the BM (e.g. Guy et al., 2011; Schulmann et al., 2014, 2009; Žák et al., 2009 and references therein) stress the importance of eastward-oriented subduction (~385 Ma to ~354 Ma) of the Saxothuringian ocean/unit beneath the eastern continental plate (represented by the Teplá-Barrandian and Moldanubian units), later accompanied by the evolution of an Andean-type magmatic arc (represented by the Central Bohemian Plutonic Complex). Collision culminated between ~354 Ma and 335 Ma and resulted in crustal thickening (~60 km) and extensive metamorphism, followed by rapid exhumation (~335 to 315 Ma).

The *Central Bohemian Plutonic Complex* (*CBPC*; Holub et al., 1997a, 1997b) is a large composite magmatic body (3200 km$^2$) that intruded the boundary between the low-grade Teplá-Barrandian and high-grade Moldanubian blocks. The rocks range from mafic to acidic, and from calc-alkaline (oldest) and high-K to ultrapotassic (youngest); five or seven magmatic suites have been differentiated (Holub et al., 1997a). I-type to transitional I/S granite types significantly predominate over rare and volumetrically minor S-types. Magmatic crystallization ages range from ~354 Ma (calc-alkaline Sázava suite; Janoušek et al., 2004) to ~346 Ma (high-K Blatná suite; Janoušek et al., 2010) for the early and main intrusive phases, and from 343 to 336 Ma (Holub et al., 1997a; Janoušek and Gerdes, 2003) for the late phases (ultrapotassic suite). The granitoid rocks that host the Mokrsko-West deposit belong to the calc-alkaline "I" type Sázava suite, i.e. the oldest suite (351 ± 11 Ma; Holub et al., 1997b; 354 ± 4 Ma; Janoušek et al., 2010). Magmatic and solid state fabrics analysis, their evolution during multiphase emplacement of the pluton and its cooling history are described in Žák et al. (2012, 2009, 2005a, 2005b).

The *Teplá-Barrandian unit* (*TBU*) represents part of the Avalonian–Cadomian belt developed along the northern active margin of Gondwana during the late Neoproterozoic (~750 to 540 Ma; e.g. Linnemann et al., 2008; von Raumer et al., 2002). The Neoproterozoic rocks (volcanic, volcano-sedimentary and flysch-type sequences) form several juxtaposed, NE–SW trending, allochthonous belts separated by shear zones, interpreted as remnants of the oceanic crust, several accretionary wedges and a single volcanic arc (Hajná et al., 2011). The intensity of the Cadomian deformation and metamorphism across the TBU decreases from the NW (amphibolite-facies) to the SE (prehnite–pumpellyite facies). The Neoproterozoic basement is transgressively overlain in the northeast by Lower Cambrian to Middle Devonian sediments of the Prague Synform (e.g. Havlíček, 1981); up to 4–6 km thick).

The *Jílové Belt* (*JB*) represents the easternmost part of the TBU; the southern and central parts of the JB are enclosed by rocks of the CBPC (Fig. 1b). This is a NNE–SSW trending, 65 km long, 1 to 6 km wide belt of Neoproterozoic volcanic, subvolcanic and volcanosedimentary rocks (Fediuk, 1992; Waldhausrová, 1997, 1984). Subalkaline Na-rich metabasalts to metarhyolites significantly predominate over metatrachyandesites. Subvolcanic rocks include albite metagranite (metatrondhjemite), Na-rich leucotonalite and alaskite (Fediuk, 2004); volcanosedimentary rocks are subordinate. According to (Hajná et al., 2011), the volcanic sequences of the JB probably represent an upper section of a Cadomian volcanic arc (660–560 Ma) developed on the oceanic crust close to the continental margin.

The rocks of the JB were intruded by numerous magmatic dikes, which are of late Cadomian and more frequently Variscan age (Morávek, 1971). The rocks of the JB were affected by Cadomian low-temperature regional metamorphism corresponding to only an anchizone to epizone transition. The intrusion of the Variscan CBPC caused contact metamorphism of the JB rocks and formation of amphibole to pyroxene hornfels (within 200–500 m from the contact with the CBPC) and/or albite–epidote hornfels (up to about 2000 m from the contact; (Morávek et al., 1994). The intensity of Variscan contact metamorphism increases from the NNE towards the SSW, in parallel with increasing volume of the granitoid masses that enclose the JB.

The northern and central parts of the belt form an anticline with a shallowly plunging axis (10°–20° to the NNE/SSW) and steep axial plane. Intense metamorphic cleavage with stretching lineation is parallel to the axial plane and axis of the anticline. Their formation is now considered to be coeval with the emplacement of the Sázava tonalite (i.e. ~354 Ma, a member of the CBPC; Žák et al., 2005a, 2005b).

The JB anticline shows weak transversal undulation, represented by alternation of axial elevations and depressions (Fig. 2). According to (Morávek et al., 1994), the axial elevations themselves acted as sites of long-lived/repeated extension, as documented by the preferential occurrence of E–W trending magmatic swarms (granodiorite porphyries dikes related genetically to the CBPC) and also of E–W trending gold-bearing quartz veins (economic and noneconomic Au deposits/prospects).

### 2.2. Brief geology of studied deposits and sites

The studied ore district is located about 60 km S of Prague, near the Vltava River (Fig. 3). It represents an area with anomalous accumulation of gold resources (~140 t Au) hosted by three genetically related gold

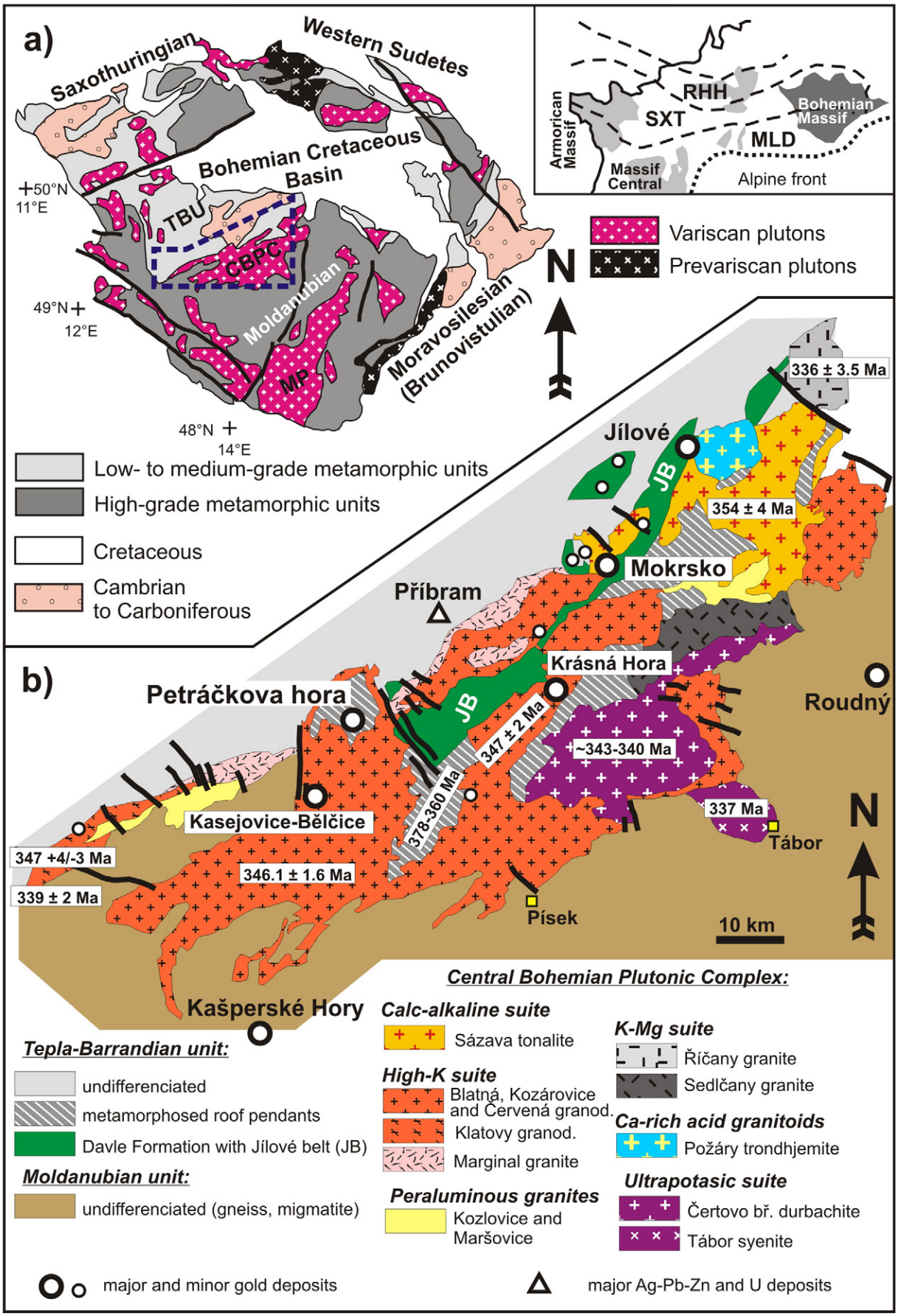
a)
Saxothuringian
Western Sudetes
Bohemian Cretaceous Basin
TBU
CBPC
Moldanubian
MP
Moravosilesian (Brunovistulian)
50°N 11°E
49°N 12°E
48°N 14°E
N
Armorican Massif
RHH
SXT
MLD
Bohemian Massif
Massif Central
Alpine front
Variscan plutons
Prevariscan plutons
Low- to medium-grade metamorphic units
High-grade metamorphic units
Cretaceous
Cambrian to Carboniferous
b)
Jílové
JB
336 ± 3.5 Ma
354 ± 4 Ma
Mokrsko
Příbram
Krásná Hora
Petráčkova hora
Roudný
347 ± 2 Ma
~343-340 Ma
378-360 Ma
337 Ma
Tábor
Kasejovice-Bělčice
347 +4/-3 Ma
346.1 ± 1.6 Ma
339 ± 2 Ma
Písek
10 km
Kašperské Hory
Central Bohemian Plutonic Complex:
Calc-alkaline suite
Sázava tonalite
High-K suite
Blatná, Kozárovice and Červená granod.
Klatovy granod.
Marginal granite
Peraluminous granites
Kozlovice and Maršovice
K-Mg suite
Říčany granite
Sedlčany granite
Ca-rich acid granitoids
Požáry trondhjemite
Ultrapotasic suite
Čertovo bř. durbachite
Tábor syenite
Tepla-Barrandian unit:
undifferenciated
metamorphosed roof pendants
Davle Formation with Jílové belt (JB)
Moldanubian unit:
undifferenciated (gneiss, migmatite)
major and minor gold deposits
major Ag-Pb-Zn and U deposits

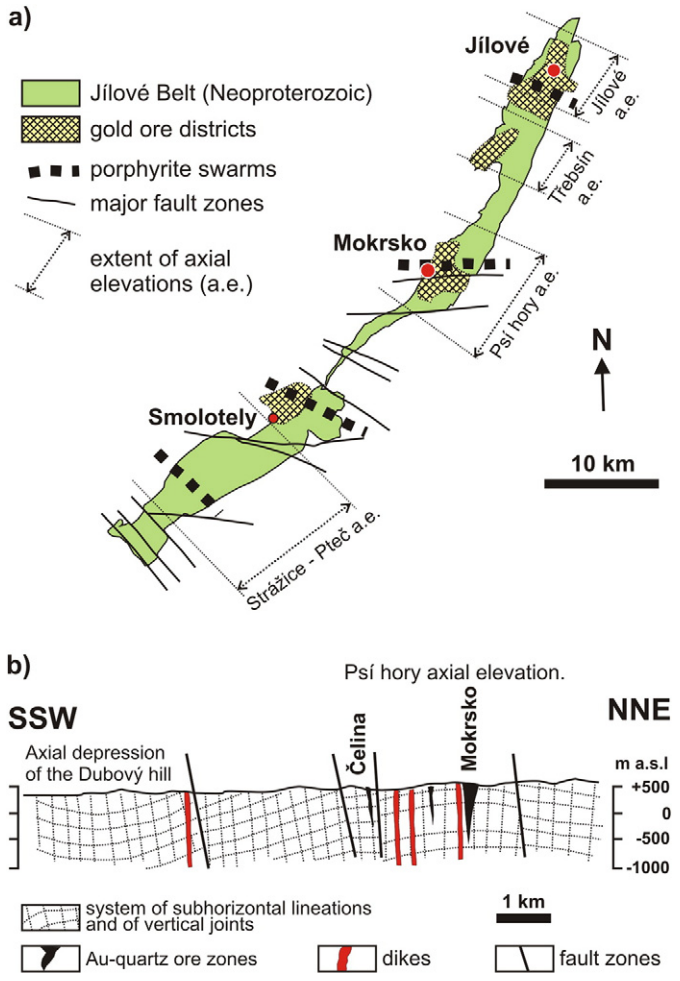


**Fig. 2.** a) Schematic distribution of gold-ore districts and of transversal structural elevations within the Jílové Belt. Note the spatial coincidence in the distribution of the gold-ore districts, the presence of E–W to NW–SE trending dike swarms of Variscan age and the transversal axial elevations (after Morávek, 1996a). b) Schematic NNE–SSW vertical section of the studied ore district, showing the structural setting of the Mokrsko and Čelina gold deposits in the transversal axial elevation (after Morávek, 1996b).

deposits: the Mokrsko-West (90–100 t Au), the Mokrsko-East (30 t Au) and the Čelina (11 t Au) deposits. They all exhibit the same E–W trending orientation of steeply dipping Au-bearing quartz veins, but they differ in their host rocks and in the thickness and spacing of the quartz veins (see below).

*2.2.1. The Mokrsko-West deposit*

The amphibole–biotite tonalite to granodiorite of the "Sázava suite" (ca. 354 ± 4 Ma; Janoušek et al., 2010) of the CBPC is the major host rock for the gold-bearing quartz veins and the ore-body at this deposit (Fig. 4). In order to distinguish the Sázava tonalite at the deposit from the same rock at other places on a regional scale, the tonalite that hosts the deposit is referred to as the Mokrsko tonalite throughout this paper.

The Mokrsko tonalite is quite homogeneous, except for small isolated bodies of leucocratic biotite granodiorite and dark diorite that have transitional contacts with it. It is almost free of mafic enclaves that are, however, quite common in the Sázava tonalite at other sites. The intrusive contact of the Mokrsko tonalite is steeply inclined (70–80° to ESE) and parallel to the trend of the JB. The intrusive contact was only weakly reactivated during late brittle tectonic phases. The Mokrsko tonalite lacks macroscopically visible evidence for intense/moderate deformation of either supersolidus or subsolidus nature. There is also no significant change in the intensity and style of deformation of the JB rocks with increasing distance outwards the Mokrsko tonalite contact.

The eastern part of the Mokrsko-West deposit (about one quarter of the ore body) is built up by the Neoproterozoic rocks of the JB: contact metamorphic slates (biotite hornfels), meta-rhyolites to meta-rhyodacites and their tuffs. Up to 1–2 m thick pegmatite and aplite dikes are frequent in an about 100 m wide exocontact zone of the Mokrsko tonalite, but are almost absent in the tonalite itself. Both the Mokrsko tonalite and the JB are crosscut by an E–W trending dike of biotite granodiorite (up to 8 m wide) and by a NW–SE trending dike of lamprophyre (minette). The former predates the Au-bearing quartz veins, while the latter postdates them.

The mineralogy of the Mokrsko-West and Mokrsko-East deposits has been described in detail by Zachariáš et al. (2014). Quartz is the main gangue mineral; sulfides usually correspond to less than 5 vol.%. The proportions of arsenopyrite, pyrrhotite and pyrite vary in relation to the host rocks (arsenopyrite dominates in the tonalite, while there is more pyrrhotite in the metabasalts) and to depth. Scheelite is a minor component of quartz veins; its content increases slightly with depth. No wolframite is present at the deposit.

*2.2.2. The Mokrsko-East deposit*

The Mokrsko-East deposit is hosted exclusively by the Neoproterozoic rocks of the JB, being dominated by felsic metatuffs and by metabasalts and their tuffs. Metarhyolites to metarhyodacites are quite minor. The deposit is crosscut by two E–W trending dikes of Variscan biotite granite that both predate the formation of the Au-bearing quartz veins. In addition to these dikes, some gabbro and diorite dikes of uncertain age (pre-Variscan?) intruded the JB. They trend mostly NNE–SSW.

The Mokrsko-East deposit occurs in the eastward continuation of the Mokrsko-West deposit. The two deposits are, however, separated by an about 400 m wide zone without veins and ore. The gold grades in the peripheral parts of both the deposits decrease gradually towards the barren zone. In addition to the host rocks, the Mokrsko-East differs from the Mokrsko-West deposit mainly in the style of veining: i) in the absence of densely spaced mm-thick sheeted quartz veinlets and ii) in the dominance of mostly 5–20 cm thick, widely spaced quartz veins. The ore zone is about 200 m wide and the average gold content in the individual sectors varied between 1.5 and 4.0 g/t Au.

*2.2.3. The Čelina deposit*

The Čelina deposit, also hosted by Neoproterozoic rocks of the JB, differs from the Mokrsko-East deposit in its higher proportion of metamorphosed mafic lavas and tuffs and in the presence of Neoproterozoic(?) metatrondhjemite (albitic metagranite) in its deeper parts.

Gold-bearing quartz veins are mostly 1 to 20 cm, rarely 50 cm thick. The ore zone is about 130 m wide; the average gold content is 1.7 g/t Au and decreases with depth (down to about 1 g/t Au at 300 to 400 m below the surface). The gold distribution is more or less regular, however, contents as high as 100 g/t Au were locally encountered (most probably due to nugget effect). Only at this deposit were macroscopic aggregates of native gold recorded.

In addition to the gold mineralization, lithologically controlled "stratiform" scheelite mineralization is hosted by mafic tuffs (up to 1 wt.% W, average grade 0.3 wt.% W). It predates the Au-bearing veins; however, its origin and age are ambiguous.

**Fig. 1.** Schematic geological maps (a) of the Bohemian Massif and (b) of the Central Bohemian Plutonic Complex (CBPC) and surrounding areas, including the Neoproterozoic Jílové Belt (JB) and the most important gold deposits. The small inset (a) shows the distribution of Variscan zones in Europe: Saxothuringian (SXT), Rhenohercynian (RHH) and Moldanubian (MLD). Other abbreviations used: Teplá-Barrandian Unit (TBU), Moldanubian Pluton (MP).

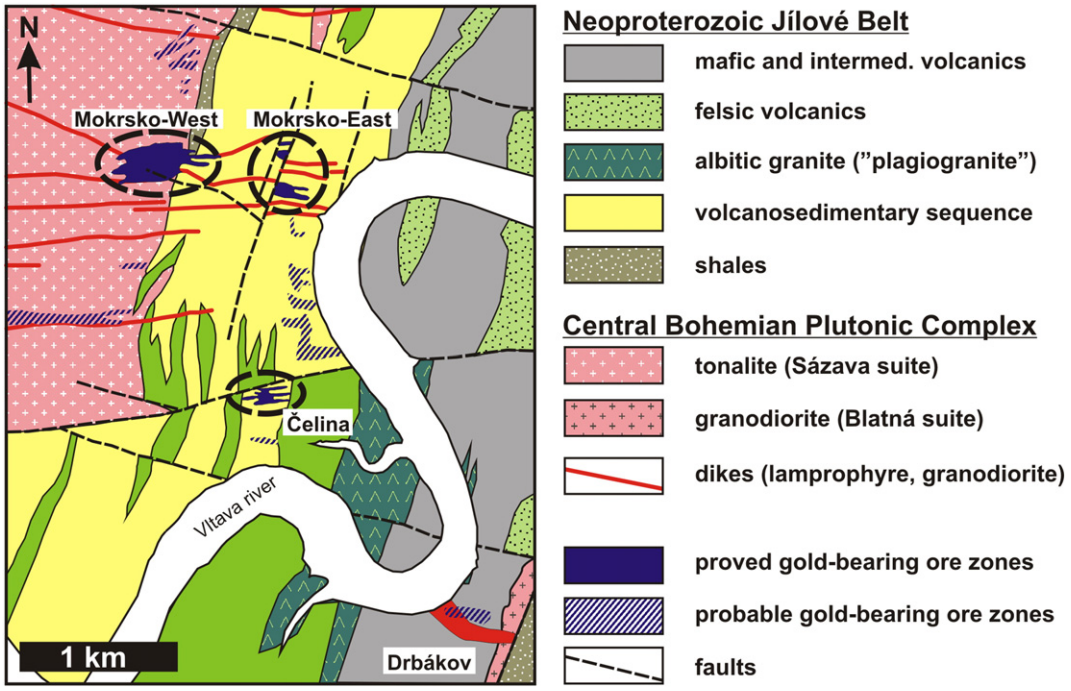


**Fig. 3.** Geology of the studied ore district and location of the Mokrsko-West, Mokrsko-East and Čelina deposits and Drbákov area (modified after Morávek, 1996b).

The structure–geology underground research was performed in the western part of the deposit as all galleries located to the E of the main adit were not allowed to enter in recent years.

*2.2.4. The Drbákov area*

The Drbákov area is located 3.5 km to the SE of the Mokrsko-West deposit, on the opposite bank of the Vltava River. It is characterized by steep cliffs with numerous discontinuous outcrops. Most quartz veins (also Au-bearing) were found to be hosted by an about 100 m wide dike of leucocratic biotite granite (related to the CBPC), striking E–W, which intruded the rocks of the JB. Surrounding JB rocks are represented by felsic and mafic metavolcanites and metatuffs with well identifiable lithological bedding. Both thick (up to 60 cm, typically less than 20 cm) and thin (mm-thick) quartz veins were found within the leucogranite dike. No quartz veins hosted by the JB rocks at the Drbákov area were found; however, they may exist.

*2.2.5. Other studied sites*

Another 26 surface outcrops distributed over an area of 5 × 15 km (Fig. 5) were studied, from the village of Živohošť in the NE to the village of Županovice in the SW, all representing the JB. Lithologically, they mostly correspond to metasediments and metabasalts, and less to metatrondhjemite.

The easternmost studied outcrop (Políčany) corresponded to the western excursion of the metamorphosed roof pendant of the CBPC, represented by weakly metamorphosed Paleozoic shists.

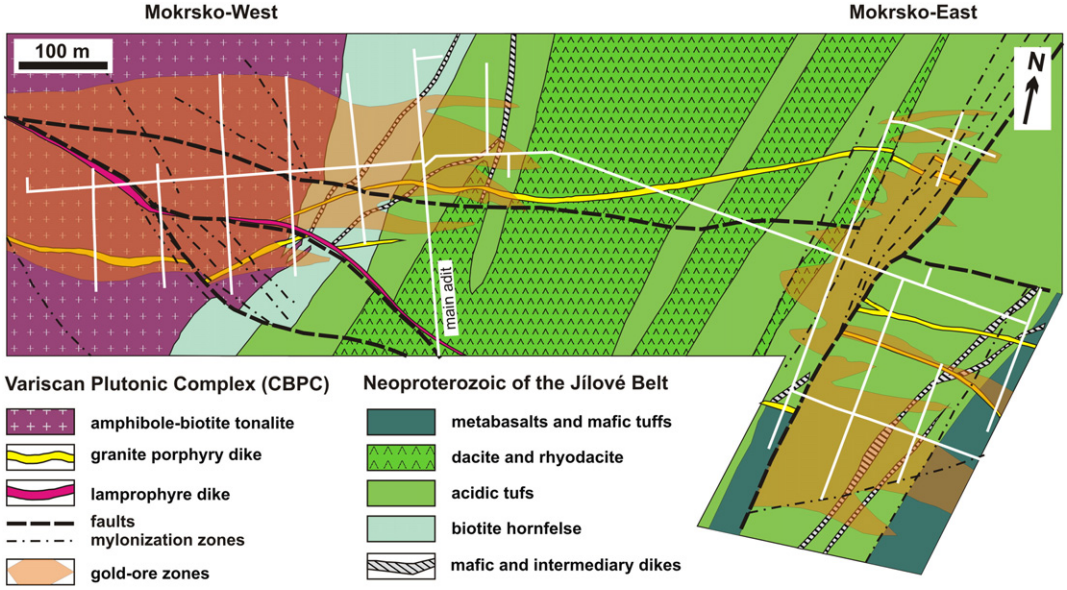


**Fig. 4.** Geological map of the Mokrsko-West and Mokrsko-East deposits (modified after Morávek, 1996b; level of the exploration adit, ca. 300 m a.s.l.).

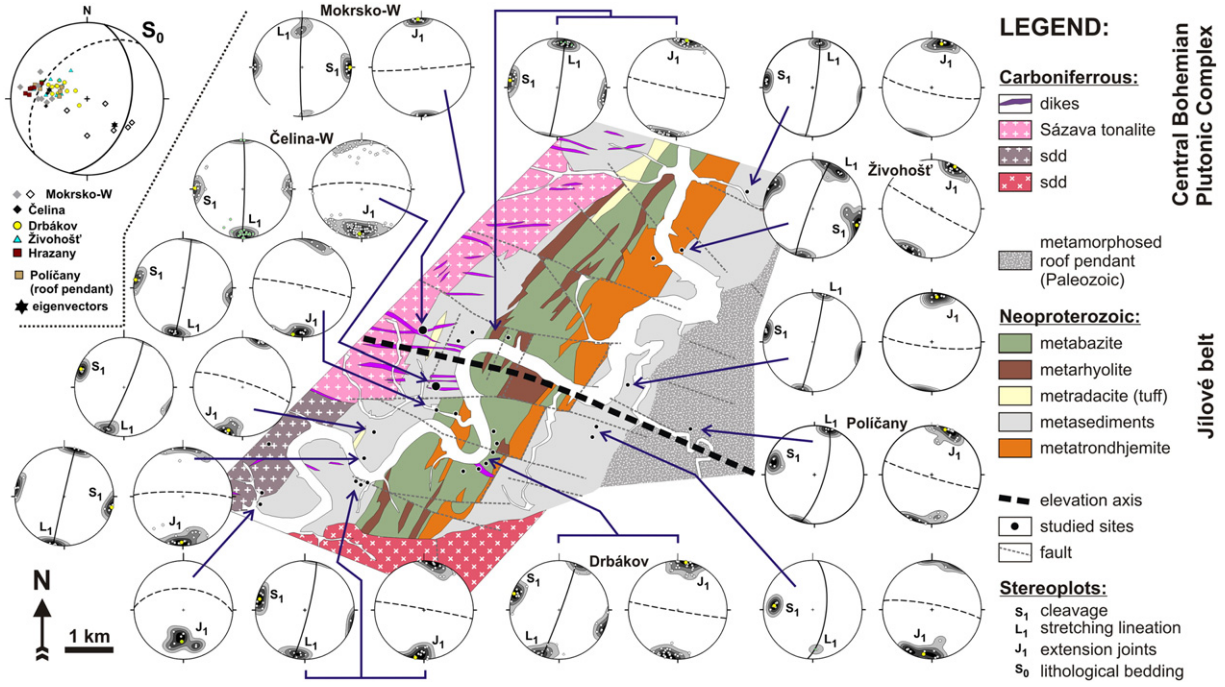


**Fig. 5.** Geology of the study area and regional variations in the orientation of the lithological bedding ($S_0$; single stereoplot in the upper left-hand corner), metamorphic cleavage ($S_1$) and lineation ($L_1$) and of $J_1$ extension joints. The axis of local transversal axial elevation is indicated by a thick dashed line. The axis of the JB anticline trends parallel with the belt, i.e. NNE–SSW.

## 3. Methods

This study is based on structural–geological research, carried out by the author underground in the Mokrsko-West and Čelina (western part only) deposits and was later extended to surface outcrops (area 5 × 15 km). Access to some parts of underground galleries is not permitted at the present time (all of those at the Mokrsko-East deposit and in the eastern part of the Čelina deposit). Data for these areas were therefore excerpted from primary geological documentation from the period of exploration (Morávek et al., 1991a, 1991b, 1990). However, the author visited all these now inaccessible galleries in the past.

The following methods were employed: i) orientation and kinematic analysis of mesoscopic structures, ii) paleostress analysis of fault-slip data; iii) analysis of microscopic textures of quartz veins, and iv) distribution of veins and fractures.

Orientation and statistical analysis of structural data was performed using the Stereo 32 software. All stereoplots represent lower hemisphere equal area projection. Data for planar elements are presented as the azimuth of dip line/dip (e.g. 314°/41°).

Paleostress analysis of fault-slip data was performed using the numerical Gauss method (Žalohar and Vrabec, 2007); the data were processed in the T-Tecto software (version 3.0; author J. Žalohar).

Vein and fracture dimensions were measured systematically where possible. All the line profiles were oriented N–S (i.e. perpendicular to the strike of the studied veins and fractures). The data were measured directly in the field ($Q_{1-2}$ veins, Mokrsko-W, Čelina-W), or obtained by manual pre-processing of photographs, followed by image analysis using ImageJ software. Individual photographs represented 0.3–1 m wide segments of weathered surfaces of N–S trending joints. These sites represented the only surfaces where unambiguous identification of tiny $Q_2$ veinlets was possible. Some data were excerpted from unpublished primary geological documentation (eastern part of the Čelina dep., Mokrsko-East dep.).

Major mesoscopic structural elements (e.g. cleavage, joints, and dikes) that do not vary substantially across the whole studied area are presented collectively for all the studied sites. More detailed description is reserved only for hydrothermal veins, in order to encompass subtle differences in the style of veining at individual sites.

## 4. Results

### 4.1. Lithological bedding ($S_0$) and folding of the Jílové Belt

The northern part of the Neoproterozoic Jílové Belt (JB) near the town of Jílové/Jílové deposit (i.e. outside the study area) is formed by a NNE–SSW trending anticline (i.e. parallel to the strike of the JB), whose axis plunges ca. 10° to the NNE and whose axial plane is steep. The dip of the volcano-sedimentary strata on both flanks of the anticline varies mostly from 30° to 50° (e.g. Morávek, 1971; Morávek et al., 1994; Zachariáš et al., 2013).

However, in the study area the JB strata dip uniformly at 30°–70° to the ESE–SE. The mean orientation of the lithological bedding ($S_0$) is 103°/42° (Fig. 5; solid line). This holds not only for all sites along the eastern margin of the JB (i.e., Živohošť, Hrazany, Drbákov), and for the metamorphosed roof pendant (Políčany), but also for the central (Čelina dep.) and eastern (Mokrsko-West dep.) parts of the JB. A small amount of data from the underground of the Mokrsko-West deposit (measured near the contact with the Mokrsko tonalite) shows the opposite sense of dip (Fig. 5; dashed line; $S_0$ 314°/41°). The intersection of the two mean $S_0$ planes coincides well with the general plunge of the JB anticline axis in the northern part of the belt.

### 4.2. Cleavage ($S_1$), lineation ($L_1$) and ductile deformation of the Jílové Belt

The NNE–SSW trending subvertical cleavage ($S_1$; also locally referred to as "Jílové type cleavage") is the most uniform and widespread feature of the JB (Fig. 5). At the Mokrsko and Čelina deposits the cleavage strikes N–S, in contrast to the general NNE–SSW trend. The $S_1$ cleavage is accompanied by marked subhorizontal mineral stretching lineation ($L_1$). The stretching lineation is locally overprinted by intersection lineation, which is younger. The $L_1$ lineation plunges 0°–17° either to the NNE or to the SSW. The dominating sense of the plunge of $L_1$ separates the JB into transversal elevations and depressions, each about 4 to 10 km long.

### 4.3. Main joint systems

Up to seven groups of joints (referred to as $J_0$ though $J_6$) were identified, based on their orientation (Fig. 6). Relative-age relationships have been established only among some groups.

The $J_1$ joints represent the most distinct joint population. They show WNW–ESE strike and subvertical dip (75°–90° to NNE/SSW) irrespective of the rock type over whole area along the NW-margin of the CBPC (i.e. not only within the JB). They represent typical extension fractures. Spacing of $J_1$ joints varies between 1 and 2 m for main joints and between 0.2 and 0.6 m for common joints. Much finer spacing, down to <5 mm, can be identified at some sites. With reference to the JB belt-parallel anticline, the $J_1$ joints were referred to as *ac* joints (e.g. Morávek, 1971).

$J_2$ and $J_3$ joints are common within the Mokrsko tonalite but minor at other sites. The $J_2$ joints trend N–S to NNE–SSW (being subparallel to the $S_1$ cleavage within the JB), while the $J_3$ joints trend NE–SW and dip moderately to the NW.

The $J_4$ and $J_5$ joints trend NW–SE and dip at 30° or at 60° to the SE. The $J_5$ joints at Drbákov represent extension joints and, based on cross-cutting relationships, clearly postdate the formation of the $J_1$ joints and of most quartz veins ($Q_2$).

Two groups of subhorizontal to slightly inclined joints ($J_0$ and $J_6$) were distinguished within the JB. They have similar orientation, but are different in age. The $J_6$ joints visibly postdate the formation of the main quartz veins ($Q_{1-2}$, $Q_2$; Fig. 12a) at Drbákov, while the $J_0$ joints predate the formation of the quartz veins ($Q_2$; Fig. 13c) at Mokrsko-West. Distinction between $J_6$ and $J_0$ joints may be difficult at sites without quartz veins.

The observed relative-age relationships can be summarized as follows: $J_1$ and $J_0$ are the oldest joints ($J_0$ could be even older than $J_1$), $J_5$ and $J_6$ are the youngest joints (their mutual relationship is unclear), $J_3$ are younger than $J_1$ and older than $J_5$. Age of $J_2$ joints is unclear. They might be coeval with the $J_1$ joints (resulting from episodic switching between the minimum and maximum principal stresses), or older (ceasing phase of formation of the $S_1$ cleavage).

### 4.4. Dikes and veins

#### 4.4.1. Intrusive dikes

Both the tonalite and the JB rocks are crosscut by numerous Variscan dikes: 1) mostly E–W oriented up to 1–2 m thick dikes of biotite granodiorite, and thin dikes of pegmatite/aplite. The latter are frequent within the JB, in an about 100 m wide zone along the contact with the Mokrsko tonalite. No aplite/pegmatite dikes were observed within the Mokrsko tonalite itself (in the underground galleries). 2) E–W trending dikes of granite and granodiorite porphyries (up to 20 m thick); and 3) NW–SE trending lamprophyre dikes (up to 2 m thick; spessartite); they clearly postdate dikes of granite and granodiorite porphyries).

Groups 1 and 2 dikes (Fig. 7d) predate the formation of Au-bearing quartz veins ($Q_2$, see below), while the group-3 (Fig. 7f) postdates them. Intrusion of group 3 dikes is closely followed by formation of single thick (up to 0.5 m) barite–calcite vein with uneconomic Ag–Pb–Zn ores and by numerous thin calcite veins (barren).

In addition to the Variscan dikes, some gabbro and diorite dikes of uncertain pre-Variscan age are hosted by the Neoproterozoic Jílové Belt. They trend mostly NNE–SSW.

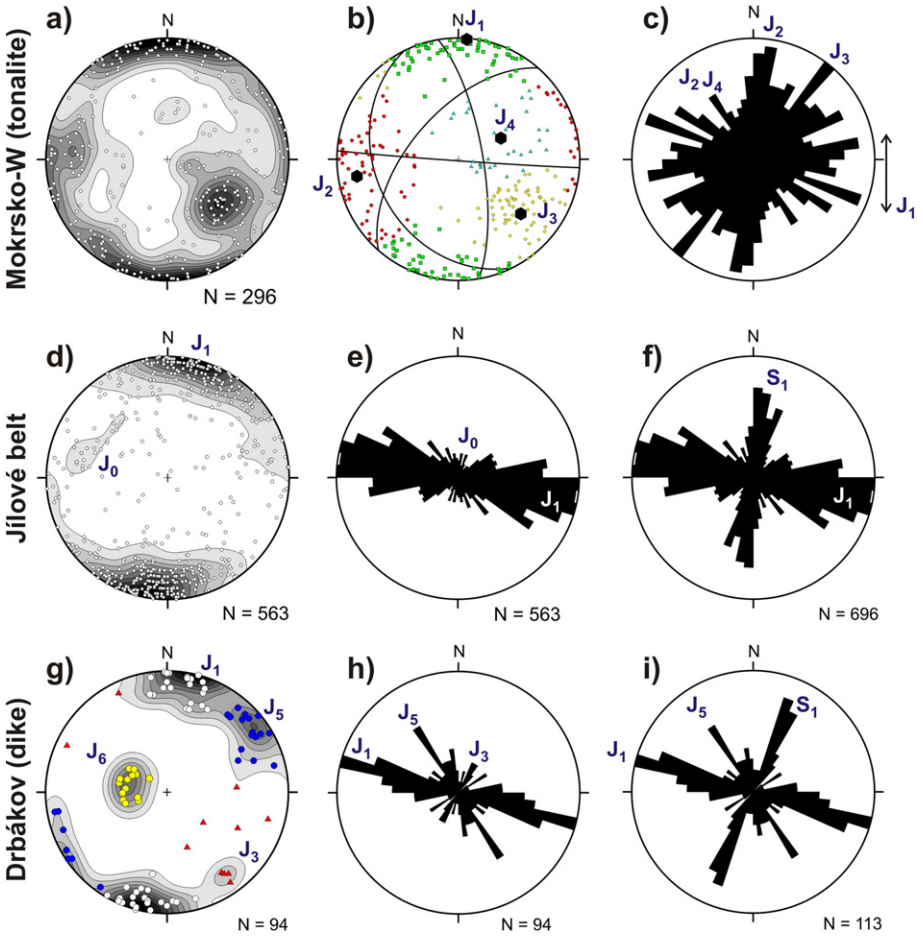


**Fig. 6.** Orientation of joints and their proposed groups ($J_0$–$J_6$): a–c) within the Mokrsko tonalite; d–f) within the Jílové belt (all studied sites); and g–i) within the dike of leucogranite at the Drbákov area. Orientation of the $S_1$ cleavage is shown for comparison on some rose diagrams.

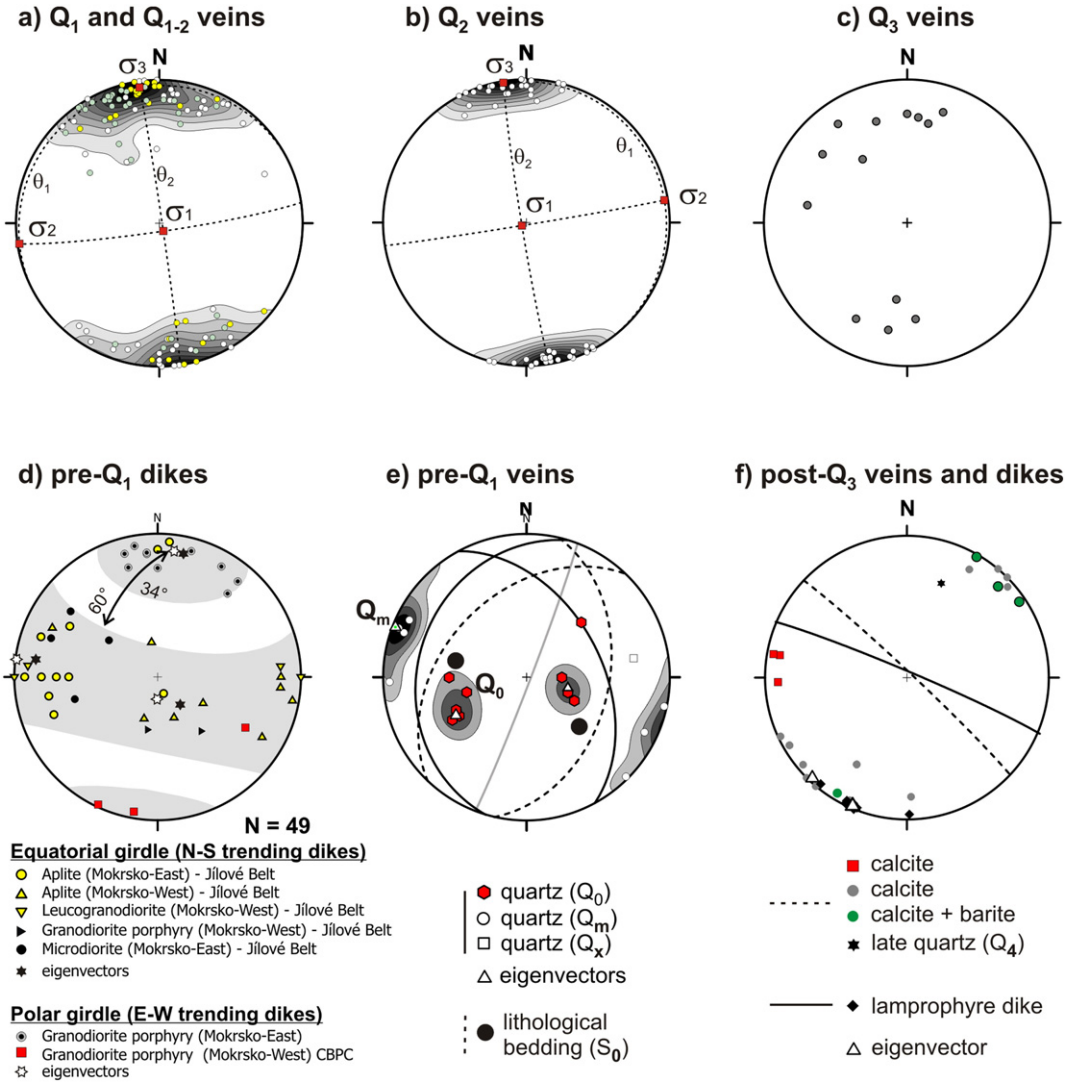


**Fig. 7.** Stereoplots of poles of veins and dikes at the Mokrsko-West deposit. Dotted lines represent supposed planes where the principal stress axes are located. Solid and dashed lines represent projection of mean planes.

*4.4.2. Quartz veins at the Mokrsko-West deposit*

Six types of quartz veins ($Q_0$, $Q_1$, $Q_{1-2}$, $Q_2$, $Q_3$, and $Q_4$; arranged chronologically from the oldest to youngest; Figs. 7-10) representing five main types of hydrothermal quartz gangue ($Q_0$, $Q_1$, $Q_2$, $Q_3$, and $Q_4$) can be distinguished at the Mokrsko-West deposit. The main ore-bearing stage is represented by the $Q_{1-2}$ and $Q_2$ veins. The Au-poor $Q_1$ veins probably occurred shortly before the main hydrothermal event ($Q_2$). The late veins ($Q_4$) are Au-barren and spatially and temporally associated with the calcite–barite vein (hosting uneconomic Ag–Pb–Zn ores). All the quartz vein types are subvertical, but $Q_0$.

The $Q_0$ veins trend NW–SE or NNE–SSW and dip moderately (20° to 50° to the NE or WNW, respectively (Fig. 7e). They are subparallel or

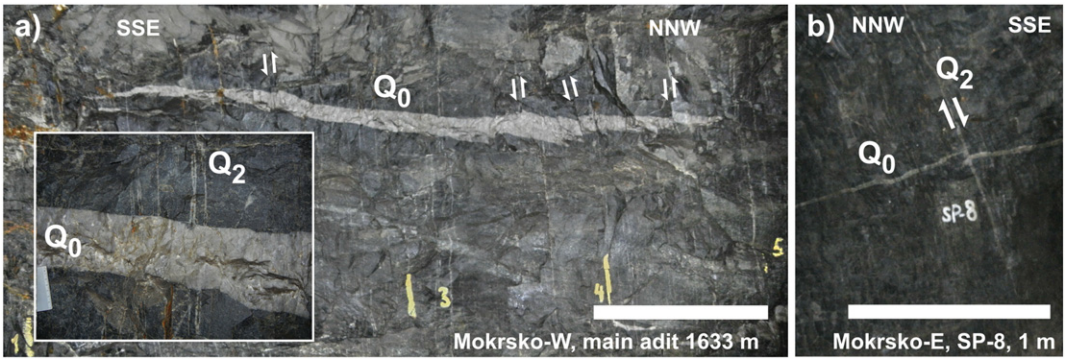


**Fig. 8.** Example of a $Q_0$ vein hosted by biotite hornfelse (scale bar = 1 m). Note that the $Q_2$ veinlets crosscut the subhorizontal $Q_0$ vein without any offset (inserted detail). Locally the $Q_0$ vein is displaced by up to 10 cm along some of the $Q_2$ veins (b). It is not clear whether this displacement is coeval with the formation of $Q_2$ veins, or it is associated with later brittle tectonic reactivation of some $Q_2$ veins.

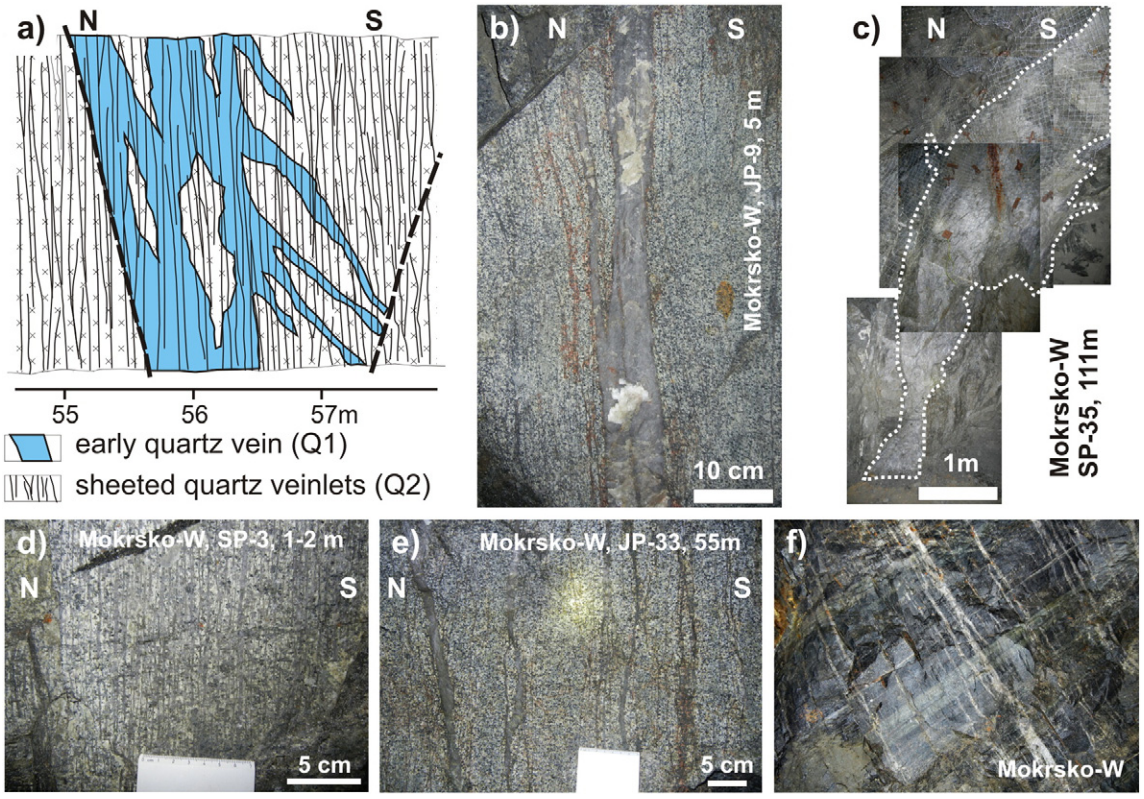


**Fig. 9.** Examples of $Q_1$, $Q_{1-2}$ and $Q_2$ veins hosted by the Mokrsko tonalite. a) Note the crosscutting of a $Q_1$ vein by mm-thick $Q_2$ veins; b) unusually thick and irregular $Q_1$ vein; c) unequivocal relationships between thicker $Q_{1-2}$ and thin $Q_2$ veins. It is possible that some $Q_{1-2}$ veins are genetically/chronologically analogous to the thin $Q_2$ veins; d) set of sheeted $Q_2$ veins in the tonalite showing more or less homogeneous thickness and spacing; e) set of sheeted $Q_2$ veins in the tonalite showing heterogeneous thickness; f) sheeted $Q_2$ veins crosscutting layers of metatuffs of the JB. Note the absence of any offset of the strata by the $Q_2$ veins. This is evidence for their pure extension nature (photo of the ceiling of the mine gallery).

slightly oblique with respect to the strike and dip of the lithological bedding (if identifiable). As they lack evidence for substantial lateral offset of the vein walls (Fig. 8), they may be considered to be mode I or mixed mode I–III fractures. They are up to 15 cm thick, of small lateral extent (<25 m along strike) and free of associated wall rock hydrothermal alteration (even when hosted by biotite hornfels). They are quite sparse. They were found at the eastern periphery of the Mokrsko-West deposit only, where they are hosted exclusively by the JB rocks (i.e. are never found within the tonalite). Two clusters of $Q_0$ veins can be distinguished (Fig. 7e): the mean orientation of veins proximal to the Mokrsko tonalite is 62°/47°, while distal veins are oriented 287°/25°.

The $Q_1$ veins strike E–W, dip 70°–90° N/S, show variable thickness (from 5 cm up to 1.5 m) and also lack associated wall rock hydrothermal alteration. Unambiguous $Q_1$ veins are more than 20 cm thick and are crosscut by mm-thick sheeted $Q_2$ veins (Fig. 9a, c). However, when quartz veins are less than 10 cm thick and/or lack visible evidence for crosscutting by the $Q_2$ veinlets (can be effectively masked by later deformation of the quartz gangue), their classification as $Q_1$ is ambiguous and they are grouped under $Q_{1-2}$ veins (Fig. 9b). The $Q_{1-2}$ veins represent about 10% of the total quartz gangue at the Mokrsko-West deposit. The eigenvector of the poles of the $Q_1$ and $Q_{1-2}$ veins is oriented 352°/5° (Fig. 7a).

The $Q_2$ veins represent most of the quartz gangue at the Mokrsko-West deposit. They have the form of sheeted veins and veinlets striking E–W and dipping 85–90° S/N (Fig. 7b). Thin quartz veinlets (0.1–5 mm thick; Fig. 9d-e) are common in the tonalite; thicker veins (up to 50 mm; Fig. 10a-b) are common in the rocks of the JB. The number of sheeted quartz veins varies from 10 to >100 per meter in the tonalite and less (5–20 per meter) in the Jílové Belt rocks. The thin $Q_2$ veinlets are difficult to identify in the fresh tonalite, but can be easily identified at the weathered surface of steep N–S trending joints that crosscut the $Q_2$ veins. The eigenvector of the $Q_2$ data is oriented 351°/1°.

The $Q_3$ veins show larger variations in strike and dip (Fig. 7c) than the $Q_2$ and $Q_{1-2}$ veins and are mostly 2 to 8 cm thick. They are hosted by brittle shear fractures that crosscut both the $Q_2$ and $Q_1$ veins and displace them by about 5–20 cm. Their gold content is unknown to date, despite the presence of sulfides (arsenopyrite, pyrrhotite or pyrite). They represent less than 0.1% of the total quartz gangue.

The $Q_4$ quartz does not form separate monomineral veins. It rims discontinuously post-$Q_3$ fractures filled in with calcite–barite gangue (see below). The $Q_4$ quartz is of dark-grayish, fine-grained appearance (resembling chalcedony) and is gold-barren.

In addition to the above hydrothermal types, scarce subvertical quartz veins of probable metamorphic origin (referred herein to as $Q_m$) were found at the eastern periphery of the Mokrsko-West deposit (i.e. within the JB). They differ from the $Q_1$–$Q_3$ veins in their strike (NNE–SSW; Fig. 7e) and in the presence of continuous alteration rims (up to 5 cm wide bleaching). They form either isolated extension veins (up to 5 cm thick), or en-echelon arrays. They are visibly crosscut by the $Q_2$ veins, which, in contrast to $Q_m$, lack any associated wall rock hydrothermal alteration.

#### 4.4.3. Late veins and dikes at the Mokrsko-West deposit

A single large up to 1–2 m thick steep dike of a lamprophyre trends NW–SE (Figs. 4 and 7f) and crosscuts both the tonalite and the JB rocks. The dike is accompanied by a fault zone accompanied/filled in by a thick calcite–barite vein (0.3–0.8 m thick). Due to the absence of lateral offset of geochemical gold-anomalies, the extensional nature of this dike is evident, as is that of the calcite–barite vein.

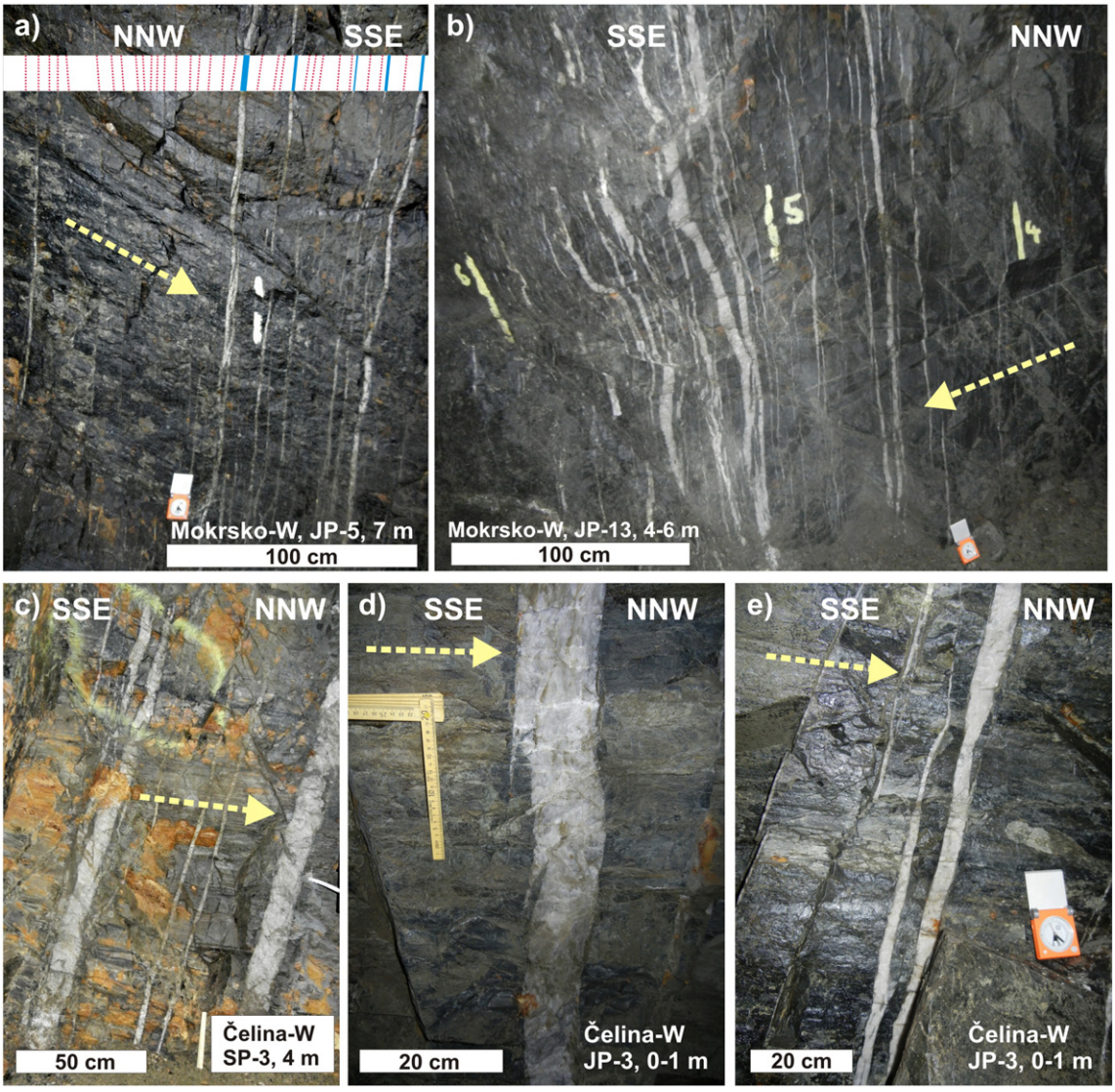


**Fig. 10.** Relationships between the $Q_2$ and $Q_{1-2}$ veins and the $J_1$ joints. The dashed arrow marks the trend of $L_1$ lineation within the plane of the $S_1$ cleavage (identical with the photo). The white strip highlights the spacing of the quartz veins (thick lines) and of the $J_1$ joints (dashed lines). Note also the increasing $Q_2$ thickness and spacing with increasing distance from the Mokrsko tonalite: (a–b: near the tonalite contact; c–e: away from the contact).

The calcite-barite vein shows massive to banded, locally brecciated texture. It is associated with sparse aggregates of pyrite, galena, sphalerite and tetrahedrite and a discontinuous rim of late quartz $Q_4$ gangue (the oldest mineral in this vein). In addition to the thick vein, numerous monomineral veins of calcite (massive texture, <5 cm thick) are present in all the studied deposits. Some of them trend N–S.

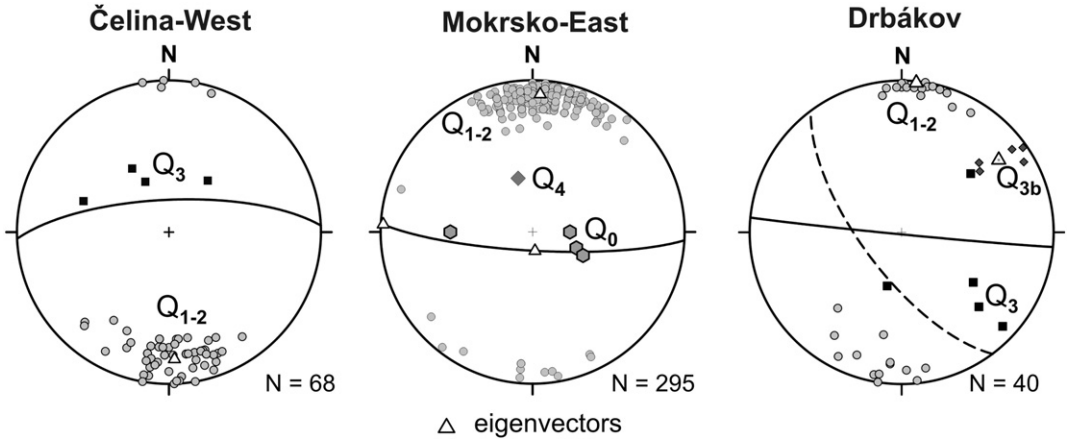


**Fig. 11.** Stereoplots of poles of quartz veins from the Mokrsko-East and Čelina deposits and from the Drbákov area. The solid lines represent the projection of the mean $Q_{1-2}$ plane, the dashed line represents the mean $Q_{3b}$ vein.

*4.4.4. Quartz veins at the Čelina and Mokrsko-East deposits*

Quartz veins at Čelina and Mokrsko-East deposit are generally much thicker (up to 90 cm) and more widely spaced than those at the Mokrsko-West deposit (Fig. 10c-e). This is related to much wider spacing of $J_1$ joints at these sites. Due to the absence of mm-thick sheeted veinlets, it is not possible to unambiguously distinguish between $Q_1$ and $Q_2$ veins at the Čelina and Mokrsko-East deposits and all the veins are referred to here as $Q_{1-2}$ type veins. Most $Q_{1-2}$ veins at Mokrsko-East dip to the N (eigenvector of poles 3°/10°), while they dip to the S at Čelina-West (the eigenvector of the poles is 178°/17°; Fig. 11).

*4.4.5. Quartz veins at the Drbákov site*

Quartz veins at Drbákov are hosted almost exclusively by an about 100 m thick dike (trending E–W) of leucocratic granite (CBPC) that intruded the JB. Most $Q_{1-2}$ veins here are >3 cm thick (up to 60 cm) and trend E–W (the eigenvector of the poles is 6°/1°; $Q_{1-2}$, Fig. 11). Some of the thicker $Q_{1-2}$ veins are accompanied by a stringer of mm-thick veinlets (Fig. 12c,e,f) resembling the sheeted $Q_2$ veins from the Mokrsko-West deposit. These are locally crosscut by moderately dipping $Q_3$ veins. Similarly to Mokrsko-West, sparse subhorizontal veins ($Q_0$) clearly represent the oldest veins (Fig. 12e). In addition to the main trend (E–W), some quartz veins also trend NW–SE (eigenvector: 53°/21°). These veins postdate the $Q_{1-2}$ veins, $J_3$ joints and also the $Q_3$ veins (Fig. 12d). Therefore they are referred to as $Q_{3b}$ veins. Their formation is probably coeval with the formation of similarly oriented $J_5$ joints.

*4.4.6. Quartz veins at other studied sites within the Jílové Belt*

Rare, steep, up to 2 cm thick E–W trending quartz veins were identified about 3 km SW of Čelina and can be classified as the $Q_{1-2}$ type and considered as the distal manifestation of the same hydrothermal system that led to the formation of the Mokrsko-West/East and Čelina deposits.

Quartz veins are practically absent over the whole studied area (5 × 15 km; except the ore deposits). At Živohošť (6 km NW from the Mokrsko-West), a single vein, about 10 cm thick and subparallel to lithological bedding ($S_0$), was found. This could be classified as $Q_0$.

*4.5. Relationship between joints and quartz veins on deposit and regional scales*

On a regional scale, local maxima of the poles of $J_1$ joints markedly coincide with the local maxima of $L_1$ lineation (Fig. 5). On an outcrop scale, notably within the JB, it is evident that most of the $Q_{1-2}$ and $Q_2$ veins fill the pre-existing $J_1$ joints. For example, at the eastern periphery

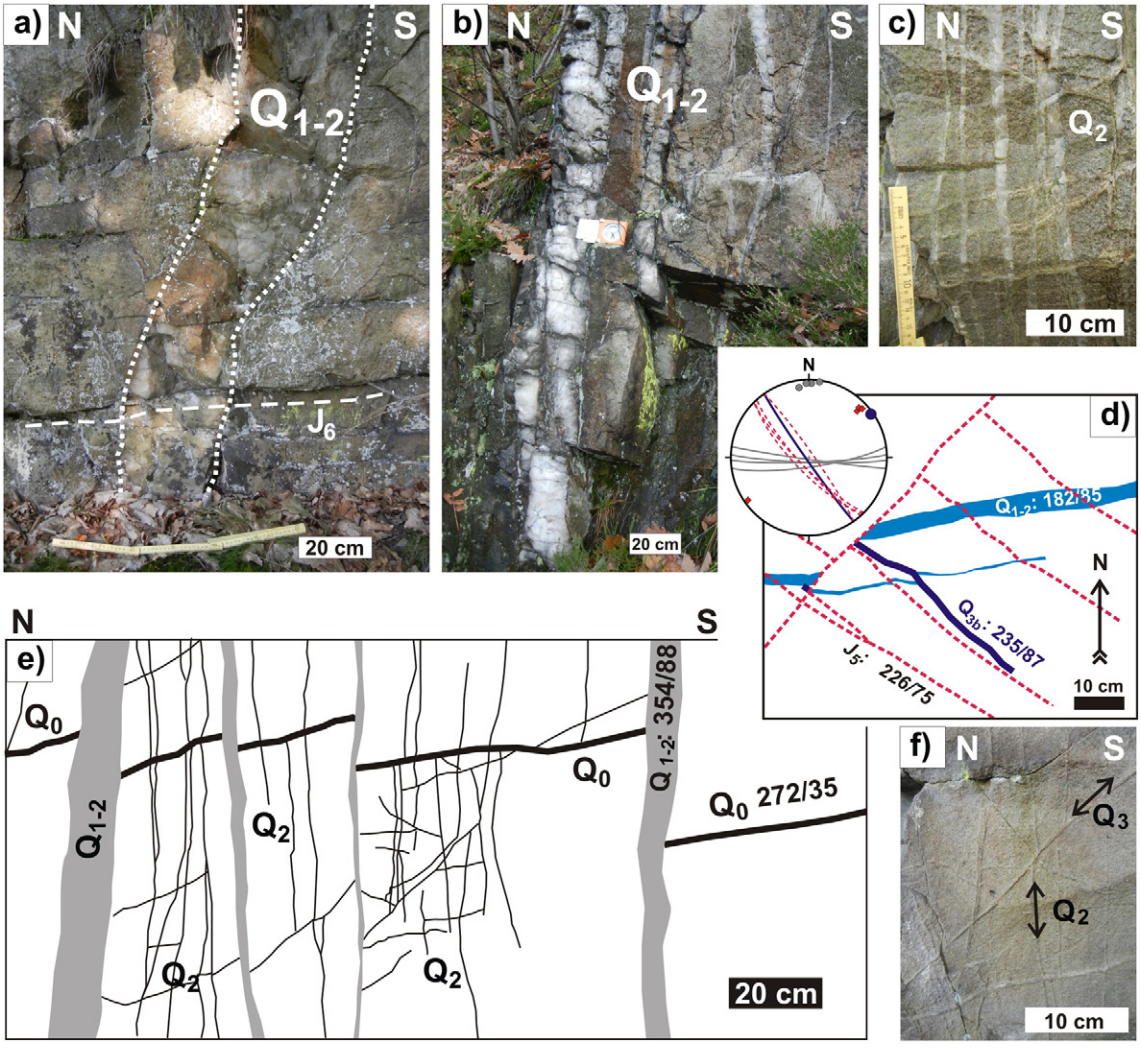


**Fig. 12.** Quartz veins at the Drbákov area, hosted by a dike of biotite leucogranite (about 100 m wide): a) Note crosscutting of the $Q_{1-2}$ vein by the $J_6$ joint; b) set of E–W trending parallel veins; c) stringer of mm-thick veinlets ($Q_2$?); d) evidence for displacement of the $Q_{1-2}$ vein by the $Q_{3b}$ vein that is parallel to the $J_5$ joints; e) the relationships between $Q_0$, $Q_{1-2}$, $Q_2$(?) and $Q_3$ (redrawn from a photo); f) detail of mm-thick veinlets from the previous scheme.

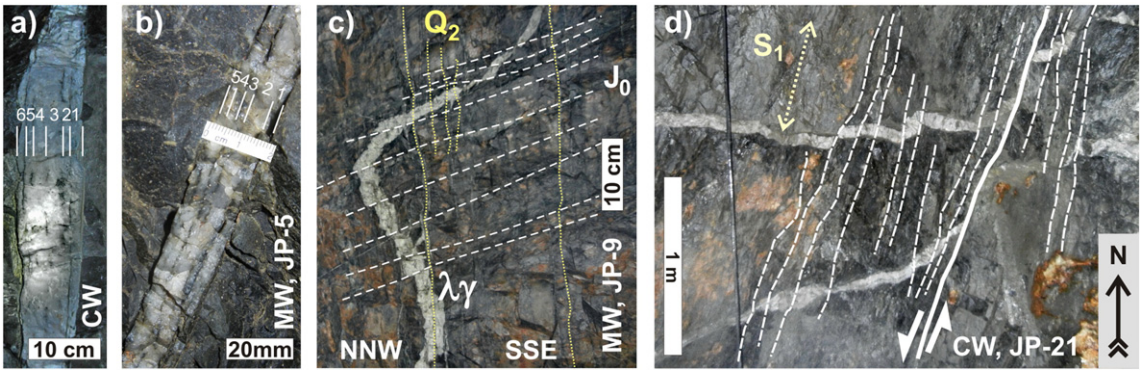


**Fig. 13.** Underground photo from the Čelina-West (CW) and Mokrsko-West (MW) deposits: a–b) quartz veins with several inclusion bands of silicate minerals implying successive opening via a crack-seal mechanism; c) thin dike of leucocratic granite systematically displaced by moderately inclined $J_0$ joints. Note that the thin $Q_2$ veins (highlighted) that crosscut both the dike and the $J_0$ joints without any visible offset must be younger than the $J_0$ joints; d) sinistral displacement of the quartz veins along fractures subparallel with the metamorphic cleavage $S_1$.

of the Mokrsko-W deposit almost all $Q_{1-2}$ and $Q_2$ veins occupy the pre-existing $J_1$ joints. However, not every $J_1$ joint is filled by the quartz gangue (Fig. 10a-b). Numerous $J_1$ joints are left closed or only a particular segment of a joint is filled with the quartz gangue. A similar pattern can be observed at the Čelina and Mokrsko-East deposits, except for wider spacing of the $J_1$ joints and $Q_{1-2}$ veins (Fig. 10c-e). The formation of the $J_1$ joints therefore represents an important step towards the formation of the ore-bearing structures.

The relative timing of the joints, dikes and quartz veins can best be studied at the eastern margin of the Mokrsko-W deposit. The Mokrsko tonalite and the JB rocks were intruded here first by an about 10 m wide dike of biotite granodiorite porphyry. The dike trends E–W and is more or less parallel to the regional trend of the $J_1$ joints. It is possible that some joints of the $J_1$ population already existed during/before intrusion of this dike. Both the porphyry dike and the JB rocks were later intruded by steep N–S trending dikes of biotite aplite to biotite leucogranite, which are only 1–15 cm wide. These dikes locally develop subhorizontal apophyses. The steep aplite–leucogranite dikes are systematically displaced by moderately dipping $J_0$ joints/fractures spaced about 10 cm apart. Subtle displacement of aplitic dikes indicates dominant reverse sense of slip along most of $J_0$ joints (Fig. 13c). Overall scarcity of pre-$Q_1$ dikes (e.g. aplite), however, does not allow to judge if the slips along $J_0$ joints/fractures represent widespread, or local phenomena. Similarly it is not possible to identify if the slip is coeval with the fracture formation (i.e. shear fracture), or if it is younger (i.e. reactivated joint). The dense network of sheeted $J_1$ joints, filled in with mm-thick $Q_2$ veins, however, is not affected by the movements along the $J_0$ joints/fractures. The $J_0$ joints/fractures are thus older than the $J_1$ ones and the formation of the dense network of $J_1$ joints and $Q_2$ veins postdates the intrusion of the granodiorite porphyry dike. Later, after minor reorientation of the regional stress-field, the $J_5$ joints were followed by the formation of $Q_{3b}$ veins at Drbákov (Fig. 12d).

### 4.6. Thickness and spacing of $Q_{1-2}$ and $Q_2$ veins

The thickness of the $Q_2$ veins hosted by the tonalite (Mokrsko-W; in total 995 veins were measured) varies from <0.1 to 15 mm; 50% of the data (1st–3rd quartiles) lie between 0.43 and 1.21 mm (Fig. 14). The median values of the thickness of the $Q_2$ veins gradually decrease across the Mokrsko-W deposit from the W towards the E (Fig. 15). The thinnest $Q_2$ veins (0.17–0.47 mm) were measured in the immediate exocontact of the tonalite, within a dike of granodiorite porphyry.

Quartz veins ($Q_2$ — $Q_{1-2}$) hosted by the JB rocks show the opposite trend. Their thickness gradually increases in the eastward direction (Fig. 14b): from 0.7–1.6 mm near the contact with the Mokrsko tonalite, to ~10–50 mm about 25–50 m away from the contact and finally to ~50–100 mm at the Mokrsko-East deposit (about 600 m away from the contact). A similar relative relationship also holds for the spacing of the $Q_2$ (Mokrsko-W) and $Q_{1-2}$ (Mokrsko-E) veins (Fig. 16).

The thickness of the $Q_{1-2}$ veins hosted by the Mokrsko tonalite varies from ~5 to ~300 mm (Fig. 14b), except for the thickest $Q_1$ vein (~1.5 m thick; Fig. 9c). The thickness of the $Q_{1-2}$ veins hosted by the JB rocks (Mokrsko-East and Čelina) varies mostly between ~5 and ~200 mm, veins ~50 to 100 mm thick are the most frequent at all the studied

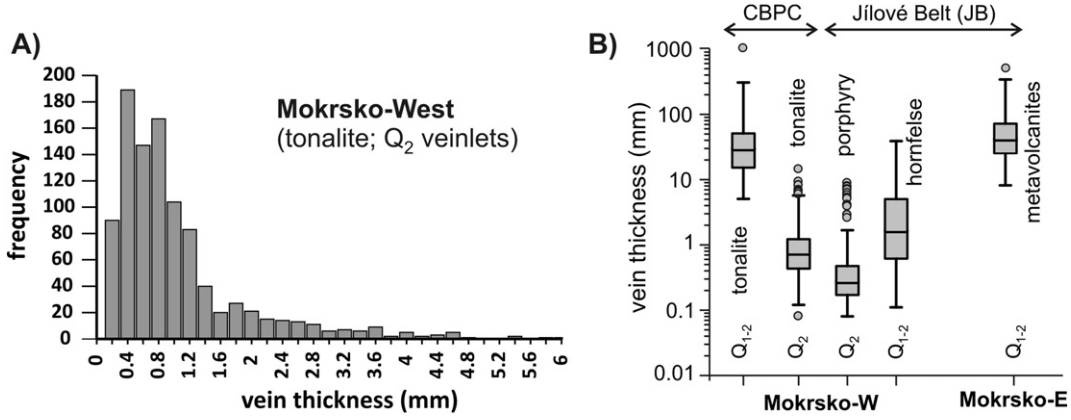


**Fig. 14.** Variations in the thickness of the quartz veins: a) $Q_2$ veins hosted by the Mokrsko tonalite; b) summary box plots for various vein types, host rocks and deposits (arranged from the W to the E).

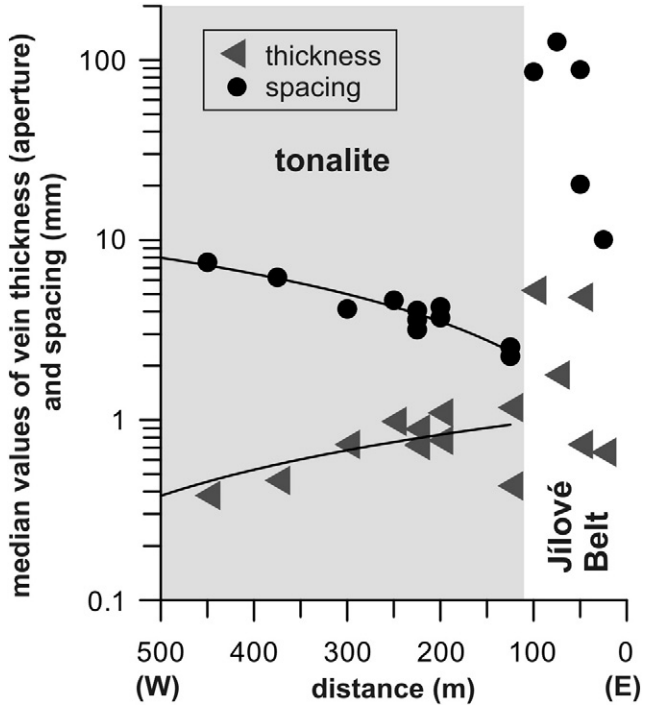


**Fig. 15.** Median values of the thickness and spacing of the $Q_2$ veins along the E–W traverse across the Mokrsko-West deposit. Note the gradual trends for both variables within the tonalite, in contrast to more scattered data within the JB rocks.

sites. The spacing of the $Q_{1-2}$ veins (thicker than 10 cm) hosted by the tonalite is ~700 mm.

### 4.7. Ellipticity of $Q_{1-2}$ and $Q_2$ veins

In order, to estimate the ellipticity (shape) of the studied veins, the vein length (L; length measured along the vein strike), vein height (H; length measured along the vein dip) and vein thickness (T), were measured both at surface outcrops and in the underground. Unfortunately it was almost impossible to measure both the L and H dimensions for a single vein. The L/H ratio is thus estimated indirectly, from the fit of L–T and H–T data. In total, only 59 data pairs were measured. These represent 34, 20 and 5 pairs of the $Q_{1-2}$, $Q_2$, and $Q_0$ veins, respectively.

It has been demonstrated by numerous studies (e.g. Schultz et al., 2013) and references therein) that dilatant fractures (veins) follow a power law relationship between the maximum thickness and the fracture length: $T_{max} = \alpha L^{\beta}$, where $\beta \approx 0.5$ and $\alpha$ is a constant that depends on the lithology. Some other authors, however, suggest $\beta \approx 1$ and linear scaling between the maximum thickness and fracture length (e.g. Olson and Schultz, 2011; Scholz, 2010). Vermilye and Scholz (1995) proposed that the value of constant $\beta$ approaches $\beta \approx 0.5$ for multi-segmented veins, while $\beta \approx 1$ for isolated (single-segment) veins. Table 1 summarizes the results of power law fits for the $Q_{1-2}$, $Q_2$, and $Q_0$ veins, undifferentiated with respect to the studied sites. Coefficient $\beta \approx 1$ is for all the veins except $Q_0$. It is common for many natural systems that the data exhibit significant scatter, caused by various factors. In our case, interaction between neighboring fractures/veins could be the most significant factor.

Based on power law fits of L–T and H–T data for the $Q_{1-2}$ veins, "average" L/H and L:H:T ratios were derived. As the vein thickness scales non-linearly with both the length and the height, the L/H ratio also varies non-linearly with the thickness: for the 5 mm thick $Q_{1-2}$ veins, the L/H ratio is equal to 1.63, for T = 20 mm L/H = 1.55, for T = 50 mm L/H = 1.50, for T = 100 mm L/H = 1.46, for T = 300 mm L/H = 1.40, and for T = 660 mm L/H = 1.36. This is in good agreement with two direct measurements of the L/H ratio (1.4 and 1.7). The $Q_{1-2}$ veins thus have the form of a horizontally elongated ellipse, whose axes ratio (L:H:T) varies from 222:139:1 to 169:124:1 for the 10 and 600 mm thick veins, respectively.

Only the H–T data are known for the $Q_2$ veins. The H/T ratio of the raw data varies from 160 to 400, the H/T ratio of the regressed data varies from 324 to 199 for the 1 and 20 mm thick veins. The L/H ratio thus remains unknown.

Few data exist for the subhorizontal $Q_0$ veins, for which the length/thickness ratio was measured only along the N–S trending profiles. Therefore it is not known which ratio (H/T or L/T) these data represent. The $Q_0$ veins exhibit the lowest ratios of all the studied quartz veins: 8 to 78, with a marked cluster at about 30.

Finally, the thickness of all the veins was plotted against their H/T or the L/T ratio (Fig. 17). Significant differences were observed: i) the H/T and L/T ratios of the $Q_{1-2}$ veins can be considered to be constant (ca. $H/T \approx 140$; i.e. they do not vary with the vein thickness); ii) the H/T ratio of the $Q_2$ veins seems, however, to increase as the vein thickness decreases; and iii) the $Q_0$ veins stay outside the trends for the $Q_{1-2}$ and $Q_2$ veins. The low amount of data, however, does not allow rigorous quantification of these trends. For example, it is ambiguous whether the H/T ratio of the $Q_2$ veins increases linearly ($R^2 = 0.35$), logarithmically

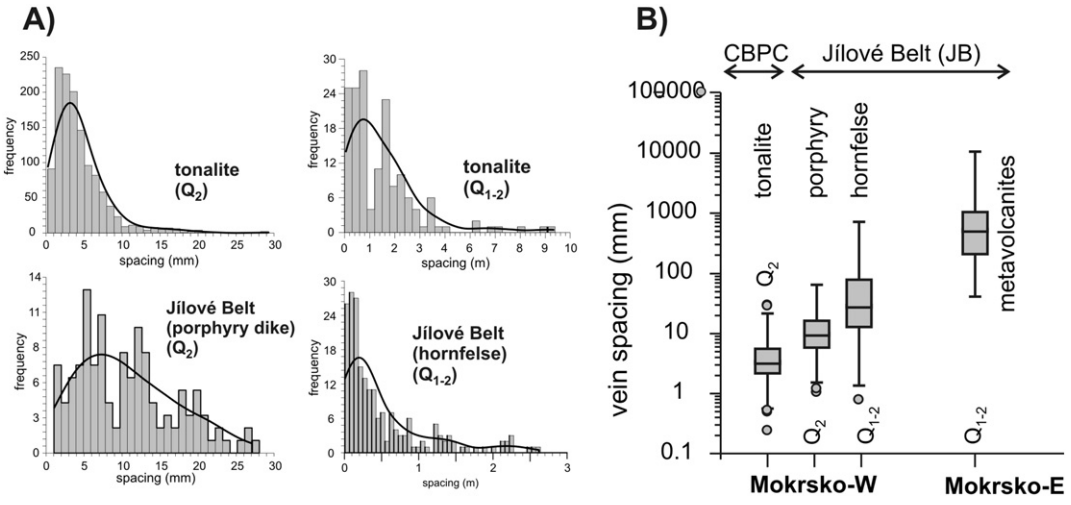


**Fig. 16.** Spacing of quartz veins: a) Mokrsko-West deposit; b) summary statistics with respect to vein type, host rocks and deposit (arranged from the W to the E).

**Table 1**
Summary of power law fits using the vein length (L), height (H) and thickness (T).

| Vein type | Power law fit ($T_{max} = \alpha X^{\beta}$) | Correlation coefficient | Profile orientation (longer axis) | Data | Mean aspect ratio (1st–3rd quartiles) |
|---|---|---|---|---|---|
| $Q_0$ | $T = 4.7617H^{0.346}$ | $R^2 = 0.761$ | Vertical (N–S) | 5 | 35 (19–51) |
| $Q_{1-2}$ | $T = 0.0073H^{1.002}$ | $R^2 = 0.974$ | Vertical (N–S) | 12 | 138 (128–149) |
| $Q_{1-2}$ | $T = 0.0033L^{1.048}$ | $R^2 = 0.979$ | Horizontal (E–W) | 5 | 196 (178–215) |
| $Q_2$ | $T = 0.0013H^{1.141}$ | $R^2 = 0.900$ | Vertical (N–S) | 16 | 285 (260–310) |

($R^2 = 0.40$) or according to the power law ($R^2 = 0.40$), as the vein thickness decreases.

### 4.8. Extension associated with $Q_{1-2}$ and $Q_2$ veins

In order to quantify the extension (fracture strain) along the E–W traverse across the ore district, local extension associated with the $Q_2$ veins was studied at 45 sites at the Mokrsko-West deposit and along a 410 m long N–S trending traverse at the Mokrsko-East deposit. The length of the studied segments was 0.3–0.7 m for the densely spaced $Q_2$ veinlets, or the full length of underground workings for veins thicker than ca 5 cm. Poor visibility of the $Q_2$ veinlets on fresh rock walls was a limiting factor for selection and the total number of studied segments.

Thick $Q_1$ and $Q_{1-2}$ veins account for about 1.5 to 3.5% of the total extension only at the Mokrsko-West deposit. Most of the extension is associated with the $Q_2$ veinlets, ranging from 3.7 up to 32% (Fig. 18). The total area occupied by the $Q_2$ gangue at the surface of the polished sample (Fig. 19; 24.8%), corresponds well to estimates based on underground photos. This seems to validate the used approach.

In general, the extension gradually decreases from the contact of the tonalite (ca. 20%) towards the tonalite interior (ca. 3–5%; towards the West) while, in opposite direction (i.e. within the JB), the extension is much lower and relatively constant (ca. 5 to 9%). The extension at the Mokrsko-East deposit, although less precisely documented, seems to be more or less constant (ca 6–8%). Finally, the extension at both deposits decreases gradually with depth (Morávek, 1996b).

### 4.9. Microtextures of quartz veins

The microtextures of the $Q_2$ veins support their extension nature by: i) the presence of rare druse cavities in the central part of the vein; ii) the absence of a lateral offset of large grains of magmatic biotite/hornblende in the tonalite host; iii) blocky-elongated quartz grains oriented more or less perpendicularly to the walls of the fracture (the same holds for rare grains of microcline, hornblende, biotite and pyrrhotite); iv) a progressive increase in the grain size of the quartz towards the core of the vein, often coupled with bilateral symmetry of the gangue; v) in contrast to other extensional veins/settings worldwide, fibrous texture of the quartz gangue was not identified.

Some of the $Q_2$ veinlets and notably almost all the $Q_{1-2}$ veins are weakly to strongly deformed on a microscopic scale. This plastic deformation of the quartz gangue is most likely a secondary phenomenon, related to the shearing of some quartz veins during the movement of rigid-blocks on a m to hundred-m scales (i.e. brittle phase deformation of the host rock). This behavior was facilitated by temperature of the host rock (ca. 300 °C). The quartz gangue thus acted as a "lubricant" in between the rigid blocks. Finally, it is common within the JB (eastern part of the Mokrsko-W deposits) that about one $Q_{1-2}$ vein per 1 to 3 m along the N–S trending profile displays visible vein-parallel displacement (about 5–30 cm; e.g. Fig. 8). This is also most probably related to subsequent rigid block movements (i.e. brittle deformation(s) postdating vein formation).

Many of the $Q_{1-2}$ and a few $Q_2$ veins show a "banded" appearance due to the presence of discontinuous lines/planes of rock-forming silicates and/or of arsenopyrite/pyrite/pyrrhotite. They resemble "crack and seal" bands, except for the thickness, which is much greater than is common (a few millimeters down to hundreds of microns in contrast to tens of microns for typical crack-seal bands). Up to 7 periods of opening and sealing can be identified (Fig. 13a-b). Typical $Q_2$ veins, however, are free of internal banding and point thus to only one opening.

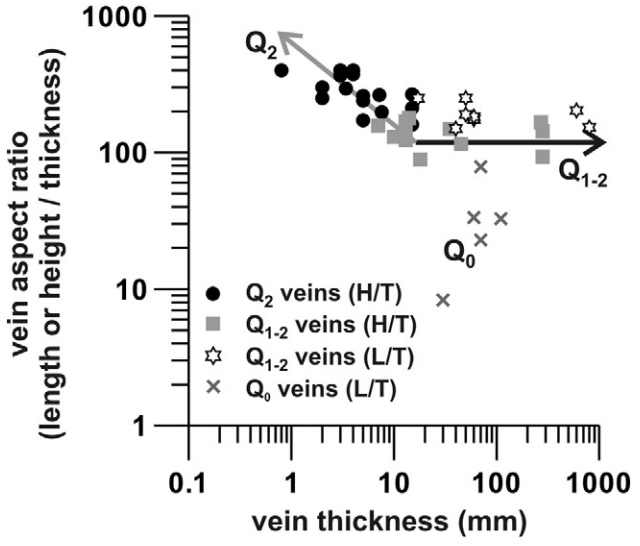


**Fig. 17.** Variations of the vein aspect ratio with respect to the vein thickness. The arrows highlight general trends.

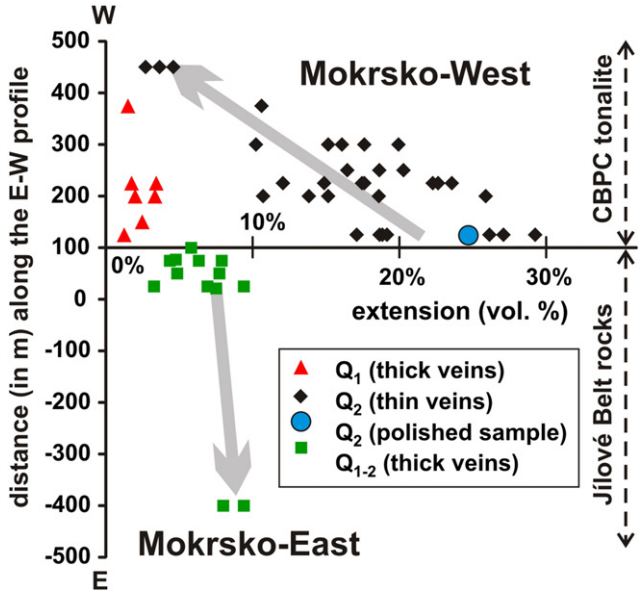


**Fig. 18.** Estimation of the extension (fracture strain) along the E–W traverse across the Mokrsko-West and Mokrsko-East deposits, based on the normalized cumulative thickness of the quartz veins. The two arrows show general trends. The extension in the tonalite is highest near its contact (25%) with the JB and decreases gradually towards its interior (4%). The extension is, however, almost constant within the JB rocks (ca 8–10%). For more details see the text.

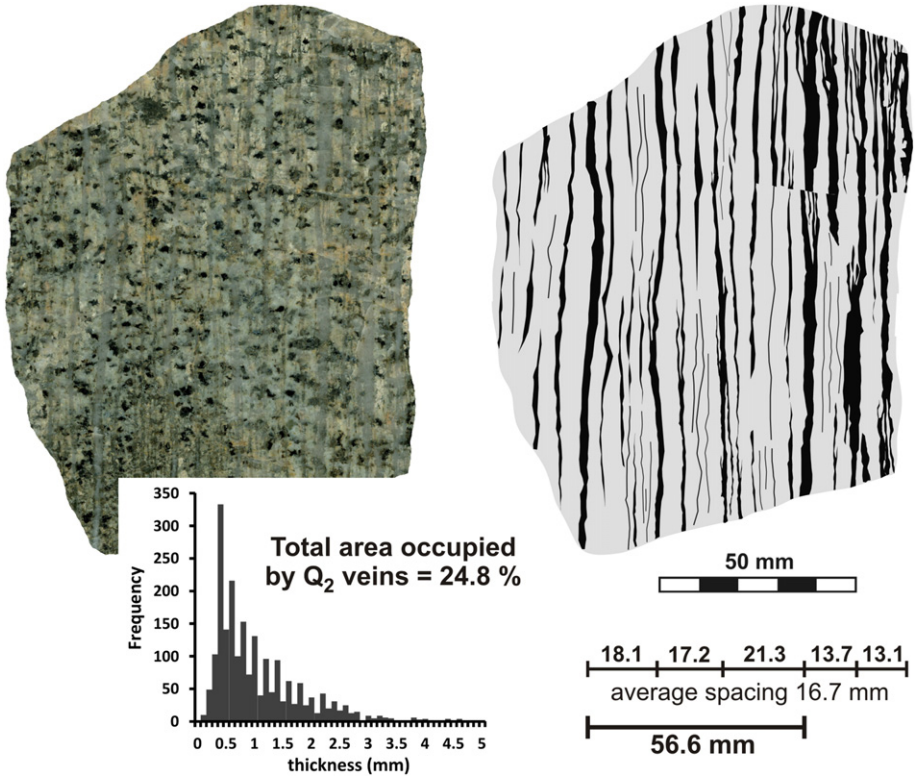


**Fig. 19.** Polished tonalite sample with dense network of thin $Q_2$ veins, photo and scheme. The veins occupy 24.8% of the total sample area. The spacing of the main $Q_2$ veins is also shown schematically.

A sample of the oldest quartz vein type ($Q_0$), collected in the exocontact zone of the Mokrsko tonalite, is almost devoid of primary fluid inclusions. This, in addition to the homogeneous grain-size reduction, indicates partial thermal recrystallization of the $Q_0$-gangue. The $Q_0$ veins may be thus older than the Mokrsko tonalite.

### *4.10. Paleostress analysis of fault-slip data*

Systematic documentation of fault-slip data at the Mokrsko-West (156 data) and Čelina-West deposits (47 data), allowed detailed interpretation of the paleostress history of brittle deformation events. Most data represent subtle fractures distributed more or less regularly within the host rock (at the adit scale of observation), few of them are related directly to major fault zones identifiable at the deposit scale. In terms of crosscutting relationships nearly all studied fractures postdate the $Q_2$ veins.

The Gauss method (Žalohar and Vrabec, 2007) of paleostress analysis was employed. Calculations were repeated until an average misfit value (15°–20°) between the theoretical and real slip vectors and numerically stable solution were obtained. The analysis resulted in the identification of three separate brittle tectonic phases (Fig. 20) differing in the orientation of the paleostress axes and in the stress ratio (represented by the D parameter, where $D = (\sigma_2 - \sigma_3) / (\sigma_1 - \sigma_3)$ and $\sigma_1$, $\sigma_2$, $\sigma_3$ are the maximum, intermediate, and minimum principal stresses).

Phase 1 represents the normal-fault regime where the $\sigma_1$ axis is vertical. The $\sigma_3$ axis is subhorizontal and oriented N–S. This phase is compatible with the orientation of the $Q_1$ through $Q_3$ veins. It is likely, that these fractures formed more or less contemporaneously with the quartz veins. Phase 2 corresponds to a strike-slip regime ($\sigma_2$ vertical) and can be subdivided into two subphases. Intrusion of the NW–SE trending lamprophyre dike associated with a thick calcite–barite vein, is compatible with phase 2 stress orientation. The same holds for the orientation of $J_5$ joints and $Q_{3b}$ veins at Drbákov. Phase 3 corresponds to the thrust-fault regime ($\sigma_3$ vertical); the maximum principal stress axis $\sigma_1$ is oriented NNE–SSW and the stress is triaxial. Orientation of $J_6$ subhorizontal joints is compatible with their formation in this phase.

Fault-slip data from the Čelina-West area has led to identification of only phases 1 and 3, with almost the same orientation and stress parameters as those for the Mokrsko-West deposit. There is also a weak evidence for phase 2b, but the amount of fault-slip data is too low.

## 5. Discussion

### *5.1. Outline of tectonic evolution of the Mokrsko ore district and of the central part of the Jílové Belt*

Structural evolution of the central part of the Bohemian Massif was from ~390 to ~350 Ma affected by tectonic stresses associated with ~NW–SE oriented subduction of the Saxothuringian plate beneath the Moldanubian plate (e.g. Guy et al., 2011; Schulmann et al., 2009; Žák et al., 2009). In this model the CBPC (ca 354–335 Ma) represents a volcano-plutonic arc of an Andean type. Although this scenario is not universally accepted (e.g. Faryad et al., 2015), it will serve as starting point of the following discussion. Actual sense of subduction is not of critical importance for our discussion, as both eastward (e.g. Schulmann et al., 2009) and westward (e.g. Faryad et al., 2015) subductions would result in similar orientation of principal stresses on a regional scale.

Regional ~NW–SE (~WNW–ENE) oriented arc-perpendicular compression related to dextral transpression (Fig. 21a) of the SE-part of the Teplá-Barrandian Unit caused initial shortening of the JB and other fore-arc units by up to 60% (Rajlich, 1988; Rajlich et al., 1988) and led to formation of the JB anticline. This deformation phase was, in its final stage, accompanied by formation of magmatic and solid state fabrics within some intrusions of the CBPC (Žák et al., 2009, 2005a, 2005b)

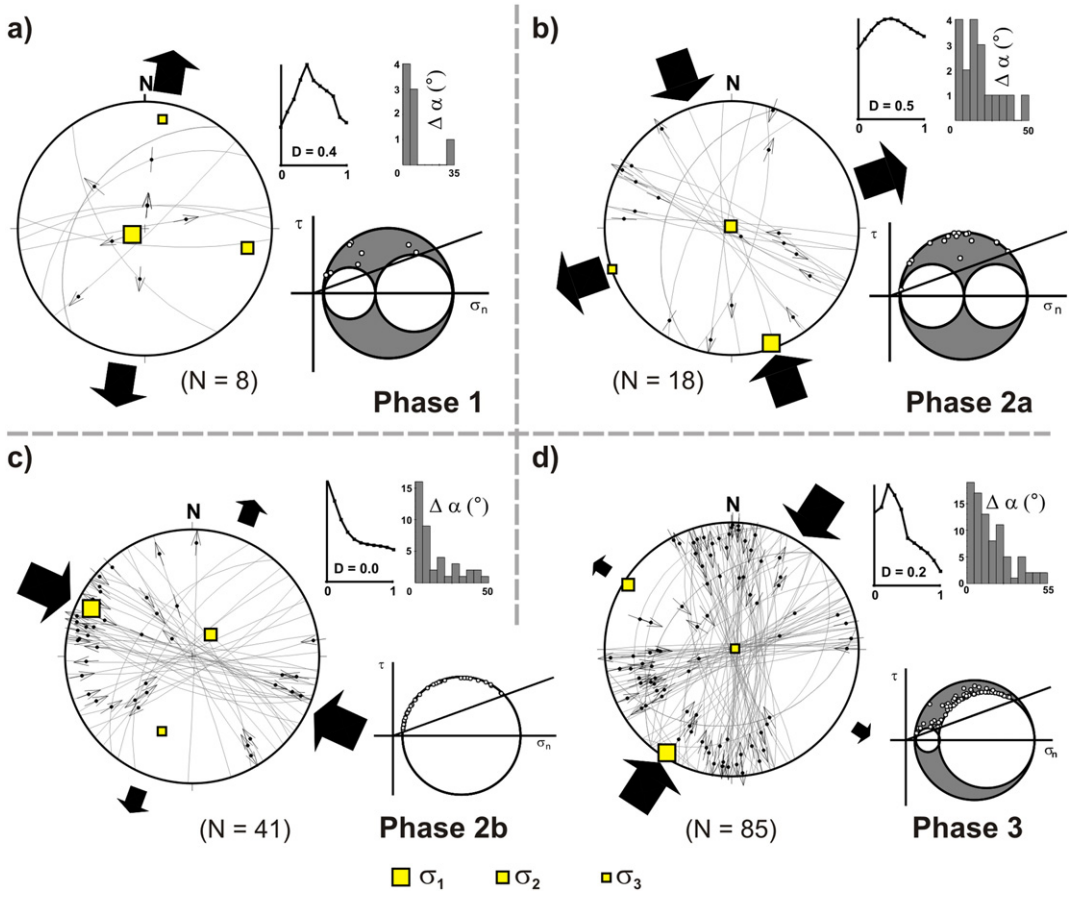


**Fig. 20.** Brittle tectonic phases based on interpretation of the fault-slip data (Mokrsko-West data set only), based on the Gauss method (Žalohar and Vrabec, 2007). The inserted graphs display the histograms of angular misfits between the calculated stress vector and the data, variation of the D parameter, and a Mohr-circle plot (relative scale).

and by intense ductile deformation of the JB ($S_1$ and $L_1$ formation). Later, during a phase of regional brittle deformation, both sinistral and dextral transpression regimes were documented along the NW-margin of the CBPC (Pitra et al., 1999).

Intense ductile deformation of the JB and formation of $S_1$ foliation and $L_1$ stretching lineation were more or less coeval with the intrusion of the Sázava tonalite (c. 354.1 ± 3.5 Ma; (Janoušek et al., 2010) as documented by similar kinematics of the ductile fabrics within the JB and

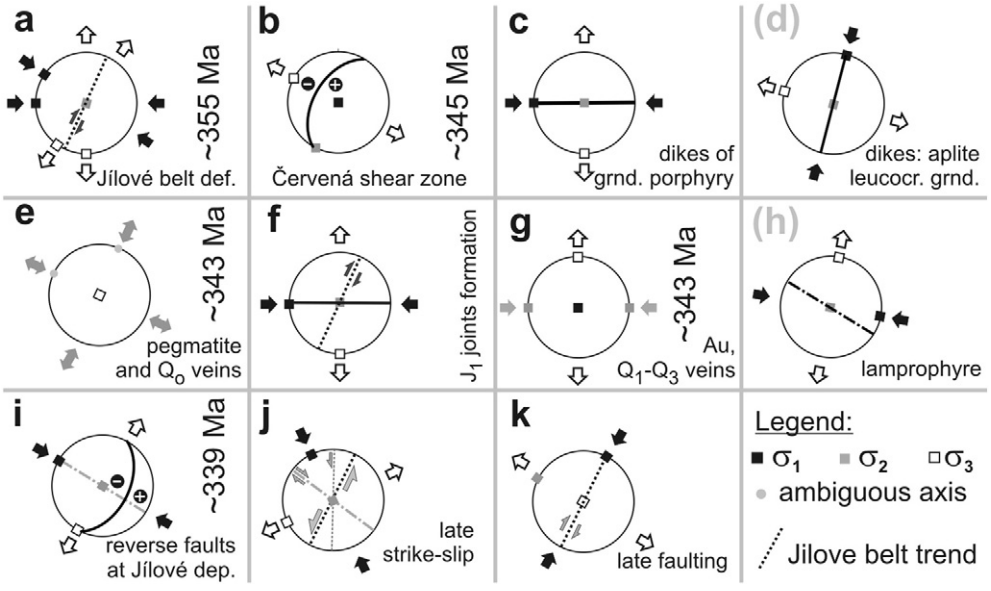


**Fig. 21.** Summary of the orientation of the principal stresses as evolved through the time in the study and related areas, involving deformation of the Jílové Belt during regional transpression (a), normal-fault regime associated with the formation of the Červená shear zone along the southeastern margin of the CBPC (b), strike-slip regimes associated with an intrusion of pre-ore dikes (c–d), compression/thrusting related to the formation of subhorizontal dikes/veins (e), dextral strike-slip regime coupled with the formation of E–W trending extensional joints (f), formation of gold-bearing veins (g), and post-Au-ore strike-slip (h–j) and compression (k) phases. See the text for a more detailed discussion.

suprasolidus (i.e. magmatic) fabrics in the endocontact zone of the Sázava tonalite (Žák et al., 2012, 2005a). The ductile deformation of the JB was facilitated by thermal softening due to the heat of the Sázava intrusion. In the study area, the Sázava intrusion flanks the JB along both its southeastern and northwestern contacts and we can speculate that the tonalite also occurs beneath the JB. This explains much the higher degree of contact metamorphism of the JB in the study area than in northern parts of the JB.

Brittle joints within the JB must be younger than the ductile phenomena ($S_1$, $L_1$). Coincidence of the maxima of the poles of the $J_1$ joints with the maxima of the $L_1$ lineation on a regional scale, as documented in this study, however, indicates that both the ductile ($S_1$, $L_1$) and brittle ($J_1$, $J_2$, $J_0$ joints) structures developed under similar stress fields, initially in ductile conditions, transitioning to brittle deformation with the cooling of the Sázava intrusion.

The next major step in the evolution of the CBPC corresponds to the intrusion of the Blatná suite (ca 347–348 Ma). Two major plutons of this suite, the Blatná and Kozárovice granodiorites, intruded at 346.1 ± 1.6 Ma and 346.7 ± 1.6 Ma, respectively (Janoušek et al., 2010). Towards the S and SE, the Blatná granodiorite grades into the Červená granodiorite (often interpreted as a more mafic variety of the Blatná type), which further to the SE is in contact with migmatites of the Moldanubian Unit. The Kozárovice and Blatná granodiorites are dominated by the NNE–SSW to NE–W steep magmatic foliation coupled with the NNE–SSW to NE–SW subhorizontal lineation, both similar to that in the Sázava tonalite. The NW–SE compression to dextral transpression therefore lasted until ~346 Ma. In contrast, the Červená granodiorite exhibits N- to NW-dipping high-temperature subsolidus foliation associated with the NW-trending (i.e. down-dip) to N-trending (i.e. dip-oblique) lineation and normal kinematics (Teplá-Barrandian and CBPC down, Moldanubian up; Žák et al., 2012, 2005a). This zone is referred to as the Červená shear zone. At ~345 Ma a switch therefore occurred from a transpressional to a transtensional regime (Fig. 21b).

Another important regional tectonic event consists in intrusions of ~W–E to ~WNW–ESE oriented steep dikes and dike swarms of granite and granodiorite porphyries (predominant), aplites and leucogranites. Most of them postdate the Blatná intrusion (ca 345–347 Ma). Their formation implies ~N–S to ~NNE–SSW oriented minimum principal stress (Fig. 21c). None of these dikes has been dated by modern geochronological methods. It may not be excluded that some of the dikes crosscutting the Sázava tonalite could be older than similar dikes hosted by the Blatná and Kozárovice granodiorites. At another intrusion-related gold deposit in the area of the CBPC, the Petráčkova hora deposit, dikes of granodiorite porphyries predate intrusion of the granodiorite stock (Zachariáš et al., 2001). They both, however, exhibit geochemical affiliation to the Blatná suite.

The NNE–SSW to N–S trending dikes of leucocratic granodiorite and aplite identified at the Mokrsko deposit may indicate a local and probably only short-term change to NNE–SSW (i.e. arc-parallel) compression and arc-perpendicular extension (Fig. 21d). We can speculate that the enigmatic subtle transversal undulation of the JB (i.e. transversal elevations and depressions; Fig. 2) formed at this stage. On a regional scale, an extensive swarm of steep diabase dikes exists within the Teplá-Barrandien Unit, near Příbram, about 5 km to the W/NW of the NW-margin of the CBPC. The dikes trend ~N–S and form a cluster spread along the NE–SW trending "Jílové fault". Formation of both the fault and dikes under the same stress orientation is probable, pointing to E–W trending minimum principal stress, N–S oriented maximum principal stress and sinistral slip on the Jílové Fault (Rajlich, 1993, 1988). The diabase dikes have not been dated yet; however, they intruded into the already folded Neoproterozoic and Paleozoic rocks of the Teplá-Barrandian Unit.

Weakly dipping $J_0$ joints that offset systematically dikes of the leucogranite at the Mokrsko-West deposit and shallowly dipping quartz veins ($Q_0$) mark the onset of a new brittle tectonic phase dominated by a subvertical $\sigma_3$ stress axis (thrust-fault regime). The orientation of other stress axes is, however, ambiguous: at some places within the JB, $\sigma_1$ seems oriented NW–SE, while at other places it is oriented NE–SW. This ambiguity on a regional scale could indicate $\sigma_1 \approx \sigma_2 \gg \sigma_3$. Similar paleostress conditions ($\sigma_3$ vertical) are compatible with the formation of subhorizontal lenses of granite pegmatite at Skalsko near Jílové (Morávek et al., 2010). Molybdenite associated with this pegmatite was recently dated to 341.3 ± 2.2 Ma (Re–Os; L. Ackerman, personal communication) and is thus about 12 Ma younger than the Sázava tonalite that hosts this pegmatite. Molybdenite from the steep E–W trending gold-bearing quartz veins at the Mokrsko-East deposit yielded a slightly older age (342.9 ± 1.4 Ma Re–Os; Zachariáš and Stein, 2001), but is still about 11 Ma younger than the Sázava tonalite. This compressive brittle tectonic phase (Fig. 21e) can thus be bracketed at ca 344–341 Ma. The presence of systematic $J_0$-like joints at the SE-margin of the Teplá-Barrandian Unit that crosscut the $S_1$-clevage and the diabase dikes supports the relative-age relationships presented in this study.

Extensional joints $J_1$ predate the gold-bearing quartz veins ($Q_1$, $Q_{1-2}$, $Q_2$). Orientations of $J_1$ and of associated fractures (see below) are compatible with a strike-slip stress regime and hypothetical dextral movements along the NW-margin of the CBPC (Fig. 21f). This phase of dextral transpression may thus represent a final phase of the main transpression event (Fig. 21a).

Paleostress analysis of fault-slip data from the Mokrsko-West and Čelina deposits revealed three main phases of late brittle deformation (Fig. 20). Phase 1 (normal-fault regime; Figs. 20a and 21g) is compatible with the orientation of the $Q_1$ through $Q_3$ veins (Fig. 7a-b). The recorded slip movements, however, may slightly postdate most of the $Q_2$ veins.

The Phases 2a and 2b (strike-slip regime; Figs. 20b-c) comprise intrusion of the WNW–ESE trending lamprophyre dike (Fig. 21h) postdates the $Q_3$ veins, followed by the formation of calcite–barite and calcite veins (locally accompanied by mineralogical occurrence of Ag–Pb–Zn phases) and by later dextral shearing of the lamprophyre dike and sinistral slips parallel with the trend of the Jílové Belt (Fig. 21j). Numerous small-scale subhorizontal slips on pre-existing fractures that are subparallel to the $S_1$ cleavage (Fig. 13d) or crosscut it at low angles, occurred at this stage also.

Strictly from geometrical aspects, the formation of reverse faults (Fig. 21i) at the Jílové district (trending NNE–SSW, dipping 40°–50° to SE) that host up to 2 m thick gold-bearing quartz veins is kinematically compatible with brittle Phase 2b (Fig. 20c). White micas associated with these veins (reverse faults) were dated to 339.0 ± 1.5 Ma (Ar–Ar; Zachariáš et al., 2013).

The last brittle phase, Phase 3 (thrust-fault regime; Fig. 20d) documents late compression subparallel to the strike of the JB (Fig. 21k). A dextral offset of about 180 m along the NNE–SSW trending fault was documented at the Mokrsko-East deposit (includes offset of the lamprophyre dike; Fig. 4).

### 5.2. Nature of $J_1$ joints

The $J_1$ joints are not only the most common joints within the JB, but also represent a key structural factor in localization of most of the gold-bearing quartz veins ($Q_{1-2}$ and $Q_2$) in the studied area. As documented above, quartz veins were formed within the JB due to fluid-pressure-driven reopening of pre-existing $J_1$ joints.

Based on the morphology, the $J_1$ joints can be classified as extensional joints. They could therefore originate either as: i) pure tension fractures under tensional stress; ii) extensional fractures formed under strike-slip regime coupled with high differential stress and low fluid pressure conditions; or iii) classical mode-I hydrofractures formed under compressional stress coupled with low differential stress and high fluid pressure. The first option can be ruled out because of the large depth of the Mokrsko deposit formation (ca 5–6 km; Boiron et al., 2001) that is not compatible with the maximum depth (ca. 1 km) that can tensional fractures reach, before they change into a

shear fractures (e.g. Gudmundsson, 2011, p. 237). The second and third options are, however, very probable, but are difficult to distinguish mutually because the morphology of the both types of fractures is often similar each to other (e.g. Mandl, 2005).

Theoretically, the early fractures could have formed under conditions of high differential stress (e.g. $\sigma_D \approx 200$ MPa) and low-moderate fluid pressure. The effective maximum principal stress ($\sigma_1'$) reached a critical value — the uniaxial compressive strength (UCS; 90 to 230 MPa for most of granitic rocks) for a given rock and the effective minimum principal stress ($\sigma_3'$) was reduced to zero by low to moderate increase in the fluid pressure. Formation of vertical joints would be then induced by horizontal compression/transpression associated with a strike-slip-regime ($\sigma_2$ vertical) and the increase in the fluid pressure would reflect the build-up of high compression. Such conditions could have existed during the early and/or late transpression phases (Fig. 21a and f).

On the contrary, mode-I hydrofractures require significantly lower values of the differential stress (e.g. $\sigma_D \approx 50$ MPa or less for the Mokrsko tonalite). An increase in the fluid pressure coupled with a decrease in the differential stress could result in the switching between these two modes of formation.

As the $J_1$ joints represent extensional fractures, the maximum of their poles defines the orientation of the minimum principal stress axis ($\sigma_3$) only. The orientation of the maximum and intermediate principal stress axes is ambiguous. At some places the $J_1$ joints are associated with small shear fractures: fresh rock segments with a width of ca 1 m, enclosed between neighboring $J_1$ joints, are damaged in detail by a network of steep-parallel shear fractures (mode II), up to 20 cm long, parallel to the main $J_1$ joints, where the displacement increases from the fracture tip to its center and the displacement vector is oriented horizontally. These fractures unambiguously indicate NW–SE to WNW–ESE horizontal orientation of the $\sigma_1$ axis. The $\sigma_2$ axis must then be subvertical.

Local variations in the strike, dip and relative-age relationships of the $J_1$ joints indicate their formation over a prolonged period. Surprisingly, the fluids that assisted in their formation left little evidence of their activity: only thin coatings of chlorite/epidote/albite are locally present. Overall uniformity of the regional distribution of the $J_1$ joints implies that they do not represent a local phenomenon. Their formation may be thus related to thermal devolatilization along the contact zone of the CBPC (the probable cause of elevated fluid pressure), coupled with long-term (~390 to ~345 Ma) ~ NW–SE oriented compression due to the subduction of the Saxothuringian plate beneath the Moldanubian plate. It is reasonable to expect that both the rate of subduction and magnitudes of the regional stresses varied through time and space, as is common in young subduction settings (e.g. Sibson and Rowland, 2003; Sibson, 2013, 2007).

### 5.3. Formation of quartz veins

#### 5.3.1. Internal structures of quartz veins

Three basic types of internal structures of the quartz gangue were identified: i) pure extensional fractures (mode I) that resulted from a single-opening event. This is valid for about half of the $Q_2$ veinlets within the tonalite; ii) veins that show evidence of several separated events of fracture-opening followed by quartz-precipitation (most $Q_1$ and $Q_{1-2}$ veins, if not obliterated by later deformation and gangue recrystallization); and iii) veins that exhibit significant recrystallization of the original quartz gangue.

Quartz veins at orogenic gold deposits frequently show evidence for the crack-seal mechanism (Ramsay, 1980), which is documented by multiple cracking of the gangue. This mechanism is controlled, in addition to other factors, by lower tensile strength of the gangue material ($T_o^Q$) than the tensile strength of the host rock ($T_o^R$), such that $T_o^Q \ll T_o^R$. The reverse condition ($T_o^Q \gg T_o^R$) leads to preferential fracturing of intact rock and can finally result in the formation of a network of hair-thin sheeted veins, the spacing of which is much smaller than is predicted from linear elastic fracture mechanics (e.g. Pollard and Segall, 1987). The later process was referred to as the "crack-jump" mechanism by Caputo and Hancock (1998) as opposed to the "crack-seal" mechanism of Ramsay (1980). Another example of the "crack-jump" mechanism was described by Holland and Urai (2010).

At the Mokrsko-West deposit, the thicker veins ($Q_1$ to $Q_{1-2}$) often show evidence for multiple opening, thus pointing to $T_o^Q < T_o^R$ conditions. Individual bands ("increments") are, however, about 1 mm thick. This is about 100 times more than is common for classical crack-seal bands (usually only 10–100 mm thick; e.g. Brooks Clark et al., 1995; Cervantes and Wiltschko, 2010). This implies that the rate of fracture opening and of quartz growth were more or less in steady-state equilibrium. The $Q_2$ veins, in contrast to $Q_{1-2}$ veins, mostly display single-step opening and narrow spacing. This may imply the tensile strength relationship $T_o^Q > T_o^R$.

Two different styles of veining at the Mokrsko-West deposit, i) older widely-spaced thick veins and ii) younger closely-spaced thin veinlets, thus seem to be related to time-dependent changes in the tensile strength of the host tonalite and/or of the vein gangue.

#### 5.3.2. Vein spacing distribution

Linear elastic fracture mechanics suggests that the spacing between the individual fractures is affected by stress perturbation around the individual fractures. Fracture formation reduces the minimum principal stress and formation of a new fracture is thus impeded within a distance of a few times the size of the fracture. For example, the stress is reduced to 35, 85 and 96% of the value of a remote stress at a distance 1, 3 and 6 times the fracture length, respectively (Pollard and Segall, 1987). The spacing between fractures is thus proportional to the fracture size (the shorter length dimension) if it is unsealed. Ladeira and Price (1981) proposed that the fracture spacing is affected by fracture-induced perturbation of the fluid pressure within and around the fracture. The distance over which the fluid pressure is restored by a new fluid is a function of the hydraulic diffusivity and time.

Based on the calculations of Simpson (2000); his Fig. 7b), following the original approach of Ladeira and Price (1981), vein spacing of 5 mm and less (i. e. like within the Mokrsko tonalite) can form only if the host rock permeability is less than $10^{-22.5}$ m$^2$ and/or the time of fluid pressure restoration is less than 1 day. Larger spacing within the JB thus implies higher permeabilities (ca. $10^{-18}$ to $10^{-20}$ m$^2$ on a 1 day scale) or longer times (e.g. 10 years for a permeability of $10^{-22}$ m$^2$).

Simpson (2000) presents a model of fracture distribution at an outcrop scale based on stress perturbation in the vicinity of an underpressured fracture that is counter-balanced by a diffusion of a fluid phase into the fracture. He found that time is the most important factor that affects the type of fracture distribution. Small time values (i.e. short time intervals of fracture formation or low permeabilities of the host rock) lead to preferential accumulation of all the new fractures in the immediate vicinity of the first-formed fracture, while large time values (i.e. long time intervals of fracture formation or high permeabilities of the host rock) result in more or less homogeneously distributed fractures over whole area (i.e. the randomness of spacing distribution increases).

Low values of the fluid diffusivity (i.e. low values of the host rock permeability) coupled with a slow rate of fracture/vein nucleation thus probably represent another important factor (in addition to $T_o^Q > T_o^R$ condition) in the formation of the relatively homogeneous stockwork of densely spaced $J_1$ joints at the Mokrsko-West deposit, which was later refilled with mm-thick sheeted quartz veins.

Finally, the spacing of the thin $Q_2$ veins hosted by the tonalite (1–5 mm) is similar to the minimum values of the observed spacing of the $J_1$ joints within the JB rocks at some places in the studied region. This allows us to suggest that the network of densely-spaced $Q_2$ veins

**Table 2**
The theta angles and derived stress (Φ) and driving pressure (R′) ratios for successive generations of quartz veins in the Mokrsko region. The data are based on four independent estimations of the $\theta$ angles for each data set. The regression coefficients ($k$) describe the empirical relationships (Eq. (10)) among the differential stress ($\sigma_D$), fluid overpressure ($P_o$) and cohesion ($\tau_o$).

| Site | Vein type | Host rocks | $\theta_1$ | $\theta_2$ | Φ | R′ | $k_1$ | $k_2$ |
|---|---|---|---|---|---|---|---|---|
| MW, ME, JB | $Q_0$ | Jilove Belt | 24.6 | 46.3 | 0.58 ± 0.07 | 0.48 ± 0.05 | 2.091 | 1.860 |
| MW | $Q_1$ | Tonalite | 47.2 | 50.6 | 0.87 ± 0.05 | 0.40 ± 0.04 | 2.482 | 1.984 |
| MW | $Q_{1-2}$ | Tonalite | 38.8 | 56.7 | 0.50 ± 0.02 | 0.30 ± 0.02 | 3.313 | 2.178 |
| ME | $Q_{1-2}$ | Jilove Belt | 56.9 | 61.5 | 0.76 ± 0.06 | 0.23 ± 0.04 | 4.392 | 2.347 |
| MW | $Q_2$ | tonalite | 60.6 | 68.6 | 0.55 ± 0.05 | 0.13 ± 0.01 | 7.494 | 2.603 |

Notes: MW (Mokrsko-West), ME (Mokrsko-East), JB (Jílove Belt outside the MW and ME deposits).

within the tonalite developed either by reopening of pre-existing fractures by fluid overpressure or by hydrofracturing of "damaged" tonalite with a high density of largely not-interconnected microfractures.

*5.3.3. Relative fluid overpressure*

Relative fluid overpressure during the formation of veins by reactivation (i.e. reopening) of pre-existing fractures can be determined by the classical approach of Jolly and Sanderson (1997). This method allows determination of the driving pressure ratio ($R'$) and the stress ratio (Φ) from the orientation of the veins. The former relates the fluid overpressure ($P_o$) with respect to the total fluid pressure ($P_f$) and the magnitudes of the minimum ($\sigma_3$), intermediate ($\sigma_2$) and maximum ($\sigma_3$) principal stresses:

$$R' = (P_f - \sigma_3)/(\sigma_1 - \sigma_3) \quad (1)$$

$$P_o = (P_f - \sigma_3) \quad (2)$$

$$\Phi = (\sigma_2 - \sigma_3)/(\sigma_1 - \sigma_3) \quad (3)$$

Both ratios ($R'$, Φ) are calculated using the theta angles derived from the stereonet presentation of poles of veins (e.g. Fig. 7a-b): $\theta_1$ represents an angle between the $\sigma_2$ axis and the data (measured along the $\sigma_3 - \sigma_2$ plane), the $\theta_2$ angle represents an angle between the $\sigma_1$ axis and the data (along $\sigma_3 - \sigma_1$ plane). When $Pf < \sigma_2$ (our case), the $R'$ and Φ ratios are related to theta angles as follows:

$$R' = (1 + \cos 2\theta_2)/2 \quad (4)$$

$$\Phi = (1 + \cos 2\theta_2)/(1 + \cos 2\theta_1) \quad (5)$$

The above approach is based on two assumptions: i) all the veins represent a single population (i.e. all are contemporaneous) and ii) all the veins were formed by reopening of pre-existing fractures due to an increase in the fluid overpressure (i.e. veins formed by fracturing of intact rock should be excluded from the analysis).

The measured theta angles and calculated $R'$ and Φ values are given in Table 2. The driving pressure ratio ($R'$) is highest for the $Q_0$ veins (0.48) and gradually decreases through the $Q_1$ and $Q_{1-2}$ veins to the $Q_2$ veins (0.13). The stress ratio (Φ), however, does not vary systematically and seems to be clustered around two more or less fixed values: ≈0.55 ($Q_0$, $Q_2$, and $Q_{1-2}$ veins at the Mokrsko-West) and ≈0.82 ($Q_{1-2}$ at the Mokrsko-West and -East).

*5.3.4. Estimation of paleostress magnitudes*

In order to estimate the absolute values of the paleostress magnitudes, André et al. (2001) extended the approach of Jolly and Sanderson (1997) by a combination of the relative stress ratios (Φ, $R'$) with an empirical failure envelope and the fluid pressure ($P_f$) estimated independently from the fluid inclusion data.

Mineral, isotope and fluid inclusion thermometry suggest the formation of $Q_2$ quartz gangue at the Mokrsko-West deposit at about 400 °C (Zachariáš et al., 2014). This in combination with the density (770 kg/m$^3$) and composition of the aqueous-carbonic fluids from which the quartz precipitated points to a minimum fluid pressure of about 170–210 MPa during the $Q_2$ quartz formation. It is reasonable to expect slightly higher pressures and temperatures for the $Q_1$ veins, and slightly lower conditions (350 °C, 150 MPa) for the $Q_3$ veins. No fluid inclusion data, however, exist for them.

In contrast to (André et al., 2001), the modified Griffith criterion is used in this study:

$$\tau = 2T_o + \tan\varphi\sigma_n \quad (6)$$

where $\tau$ is the shear stress, $\sigma_n$ the normal stress, $\varphi$ represents the angle of internal friction and $T_o$ is the tensile strength. This relation suggests that the cohesion ($\tau_o$; also referred to as the cohesive or shear strength) is related to the tensile strength by $\tau_o = 2T_o$.

The stress ratio (Φ) for the $Q_2$ veins is estimated at 0.55 and the analogous stress ratio ($D$) derived for the oldest phase of brittle deformation (phase 1) reaches a value of 0.4. Therefore, a similar stress ratio (Φ = 0.5 to 0.4) is a reasonable approximation for the $Q_3$ shear veins that closely postdate the $Q_2$ veins. The poles of the $Q_3$ veins plotted on the Mohr circle (relative scale) allowed reconstruction of angle $\varphi$ at the moment of their formation (Fig. 22). It varies between 24° to 19° for Φ = 0.6 and from 27° to 20° for Φ = 0.1. Within the expected range (Φ = 0.6 to 0.4), the value $\varphi = 24°$ is a good compromise.

Estimation of a reliable value of the cohesion ($\tau_o$) is far more problematic. For application of the empirical (Hoek and Brown, 1988) criterion, an assumption about the uniaxial compressive rock strength

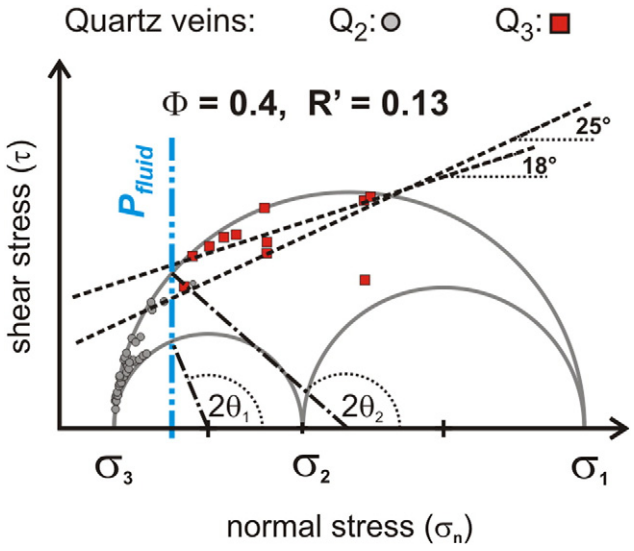


**Fig. 22.** Mohr-circle plot (relative scale) of quartz veins ($Q_2$ and $Q_3$) for given stress (Φ) and fluid (R′) ratios. The orientation of the $Q_3$ veins points to $\varphi \approx 24°$ (the average slope of the failure envelope/line). This value represents the best estimation of the angle of internal friction for the Mokrsko tonalite at the time of $Q_3$ vein formation.

(UCS) and the "quality of the rock mass" must first be made. If UCS = 210 MPa (a reliable value for the study area, see below), the cohesion varies from 25.5 MPa (intact rock) to 6.7 MPa (very good quality rock mass) and less for more fractured rock. Alternatively, the cohesion is half of those given above, if UCS = 100 MPa (common lower range of most laboratory data of granitic rocks).

The mechanical properties of granite from the CBPC can be approximated by data from an underground storage reservoir for natural gas close to Milín (about 20 km to SE from the Mokrsko): $T_o = 10.5$ MPa (tensile strength), $\tau_o = 45.4$ MPa (cohesion), $E = 83$ GPa (static Young's module), $\nu = 0.20$ (Poisson's ratio). The cohesion estimated from the empirical (Hoek and Brown, 1988) criterion, is thus at least half of the laboratory value. This may be related to a sample size effect — a common difference between the laboratory and "in-situ" data. The estimation of the paleostress magnitudes as presented below is based on the following approximations: $\varphi = 24°$, $T_o = 5.5$ and 11 MPa and $\tau_o = 2T_o$.

Fig. 23 summarizes several possible combinations of stresses during the formation of extensional veins ($Q_1$ through $Q_2$) and shear veins ($Q_3$). In all these cases, the effective normal stress ($\sigma_n'$) is plotted on the horizontal axis (i.e. the fluid pressure was subtracted). The vertical axis corresponds to the shear stress ($\tau$) and marks the relative position of the fluid pressure ($P_f$) with respect to the effective principal stresses. The first scenario (Fig. 23a) suggests the simultaneous formation of extensional and shear veins, however, by different mechanisms. The former veins were formed by reopening of pre-existing favorably oriented fractures (in our case $J_1$ joints), while the later (shear) veins were formed by fracturing of "intact" rock (as they are plotted above the failure envelope). The largest Mohr circle crosscuts the vertical axis ($\tau$) at a value equal or close to the value of $\tau_o$. The second scenario (Fig. 23b) corresponds to the minimum differential stress necessary for the initiation of shear veins. It is also compatible with the formation of extensional veins by the reopening of pre-existing fractures. The third scenario (Fig. 23c) is similar to the previous case, except for lower differential stress, such that only the formation of extensional veins is possible. In all three cases (Fig 23a-c), the stress ($\Phi$) and driving pressure ($R'$) ratios are kept constant. The fourth scenario (Fig. 23d) allows only the formation of shear veins. No pre-existing fractures can be opened/reactivated as $Pf < \sigma_3$. Note that this scenario preserves the original value of $\Phi$, but not that of $R'$. The final scenario (Fig. 23e) allows the formation of only extensional veins, however, by two different mechanisms: i) by hydrofracturing of "intact" rock and ii) by reopening of pre-existing fractures. Consequently, neither $\Phi$ nor $R'$ preserve their original values predicted by the $\theta$ angles.

The second scenario (Fig. 23b) is an appropriate model for the estimation of the maximum possible value of the differential stress ($\sigma_D$) during the formation of $Q_2$, $Q_{1-2}$, $Q_1$ and $Q_0$ extensional veins at the Mokrsko area. The actual values of $\sigma_D$ may be lower (i.e. Fig. 23c) than the maximum ones. However, a decrease in the magnitude of $\sigma_1$, must be counterbalanced by an increase in $\sigma_3$ and by a change in the magnitudes of $\sigma_2$, in order to keep the values of $R'$ and $\Phi$ constant. The second scenario (Fig. 23b) suggests:

$$\tau_o = 0.5\sigma_D \cos\varphi - \tan\varphi(\sigma_D(1 - \sin\varphi) - P_o) \quad (7)$$

$$P_o = \sigma_3 - P_f \quad (8)$$

$$\sigma_D = (\sigma_1 - \sigma_3) \quad (9)$$

Using fixed $\varphi = 24°$, $\tau_o$ can be calculated for various values of $\sigma_D$ and $P_o$. The results can be expressed in the form of empirical linear relationship between the fluid overpressure, the differential stress and the cohesion:

$$\sigma_D = k_1 * P_o \text{ and } \sigma_D = k_2 * \tau_o \quad (10)$$

Combination of these equations yields: $\tau_o = k_2/k_1 * P_o$. The values of coefficients $k_1, k_2$ are given in Table 2. Stress $\sigma_3$ (second scenario) can be calculated from:

$$\sigma_3 = 0.5k_1\, P_o(\cos\varphi - \tan\varphi + \sin\varphi\tan\varphi)/\tan\varphi + P_f - \tau_o/\tan\varphi \quad (11)$$

The paleostress magnitudes (Table 3) were calculated for two values of the tensile strength of the tonalite (5.5 and 15 MPa) and for $\tau_o = 2T_o$. The magnitudes of the principal stresses during the formation of the $Q_3$ veins were not estimated but should be higher than those estimated for the $Q_2$ veins, as the $Q_3$ veins represent shear fractures (mode-II fractures).

*5.3.5. Fluid overpressure based on vein aspect ratio*

Another approach to estimation of the fluid overpressure, based on the principles of linear elastic fracture mechanics, is related to the ratio of the fluid overpressure ($P_o$) to the vein aspect and also to the elastic properties of the host rock. For more details on this approach, see Gudmundsson (2000) and Gudmundsson et al. (2012) and references therein. In our case, the model of non-restricted mode I elliptical interior fracture is used:

$$P_o = \frac{T_{max} E\, E(\varepsilon)}{-2L(1-\nu^2)} \quad (12)$$

where $P_o$ denotes the fluid overpressure (in MPa), $T_{max}$ denotes the maximum vein thickness (in m), $L$ denotes the length (in m; the smaller dimension is used if both the length along the vein dip and the vein strike were measured), $E$ is Young's module (in MPa), $\nu$ is Poisson ratio (the value 0.25 is used in all the calculations), $E(\varepsilon)$ is the complete elliptic integral, whose value depends on the length ratio (longer dimension/smaller dimension; $L/R$) and varies from ca. 1.57 for a penny-shaped crack ($L/R = 1$; i.e. circular) to values close to unity for a highly elongated crack (i.e. elliptical cracks with $L/R > 10$). Of the variables above, the value of Young's module has the most significant effect on the calculated value of the fluid overpressure. The value of $\nu$ has a negligible effect, due to its square root.

While the dimensions and aspect ratios of most veins are known, the value of Young's module at the moment of vein formation (ca. 400 °C and 5 km depth) has to be estimated. The starting point may represent laboratory data of the granodiorite from the underground storage of natural gas near Milín ($E = 83$ GPa, $\nu = 0.20$; see above).

A Young's module ($E$) value equal to 80 GPa (the common range for granite to tonalite is 40–120 GPa) results in overpressure between 356 and 456 MPa for the $Q_{1-2}$ veins (aspect ratios 128 to 148; 25th–75th percentiles), or between 182 and 228 MPa, if $E = 40$ GPa (i.e. lower-limit of most laboratory data). The overpressure estimated for the $Q_2$ veins (aspect ratios 260–310) is slightly lower, 175–225 and 87–112 MPa, for $E = 80$ and 40 GPa, respectively.

If we wish to obtain the fluid overpressure for the $Q_{1-2}$ and $Q_2$ veins similar to the values estimated independently (i.e. 4 to 10 MPa, or 10 to 27 MPa for $T_o = 5.5$ and 15, respectively; see Table 3), the used values of $E$ should be as low as 2.2 or 5.8 GPa for the $Q_2$ veins, or 1.3 and 3.5 GPa for the $Q_{1-2}$ veins.

Laboratory values of static Young's module as low as 30 to 15 GPa are sparsely reported for some hydrothermally altered (clay-type alteration) and highly fractured granites. At the moment of formation of the quartz veins, the Mokrsko tonalite was probably almost fresh (the alteration is weak at present) and therefore the hydrothermal alteration is not the right reason for reduction of the $E$ values. This reason could be, however, a dense network of microfractures.

For igneous and metamorphic rocks, it is common that the laboratory measured values of $E$ of are up to 5 times greater than the "in situ" values. For heavily fractured and unsealed rock, this difference could be even greater. Increasing temperature, porosity and increasing water content also all decrease the value of E for a given rock (e.g.

Gudmundsson, 2004). Increasing the mean stress (and thus the depth), however, increases the value of E (e.g. the values measured at 3 kbar are ca. 1.5–2 times greater than those measured at 1 bar). If all these factors are summed up, the "in situ" value of Young's module of the Mokrsko tonalite could be as low as ≈10 GPa at the moment of vein formation.

The $Q_0$ veins differ significantly from other vein types in their very low aspect ratios (≈35; 19–51). This results in unrealistically high overpressure (>500 MPa) for $E > 40$ GPa and persisting high values (99 MPa; 68–175 MPa) if $E = 5$ GPa. This, in addition to other evidence (mineralogical, structural), suggest genetic (and temporal?) separation of $Q_0$ veins from $Q_1$ through $Q_2$ types. Alternatively, it may point to more complex history that altered the initial aspect ratios of the $Q_0$ veins (e.g. Johnston and McCaffrey, 1996).

As noted earlier (Fig. 17), the $Q_{1-2}$ veins exhibit more or less constant aspect ratios (independent on the thickness). This indicates more or less constant fluid overpressure during their formation. On the other hand, the aspect ratios of the $Q_2$ veins are inversely correlated with their thickness. The thinner and more frequent $Q_2$ veins should thus have been formed under lower fluid overpressure than the thicker ones. Fig. 24 demonstrates the relative distribution of the fluid overpressure (for $E = 5.8$ and 80 GPa) based on the thickness distribution of the $Q_2$ veins and a power law relationship ($A = 375.2\ T^{-0.211}$) between the $Q_2$ thickness (T) and the aspect ratio (A).

The variability of the vein aspect ratios is partly attributed to a data collection process (the absence of large continuous outcrops), but the major factor seems to be a variation in the fluid overpressure and/or in the value of Young's module ($E$). Similar conclusions can be drawn from variations in the vein thickness measured along the strike of the individual veins (Fig. 25). The data are compatible with constant fluid overpressure over whole length of each fracture; however, they suggest variation of the $E/P_o$ ratio (95–600) from vein to vein. It is easier to imagine that these variations were caused by variations in the fluid overpressure (it is also affected by the diffusivity of the fluid, permeability of the host rock and tectonic stress) rather than by the value of Young's module.

#### 5.3.6. Depth of the fluid source reservoir

Two different models can be employed to determine the relationship between a vein and its fluid source reservoir: i) model-1, based on the static fluid overpressure, suggests instant connection between the vein and its fluid source reservoir (e.g. Gudmundsson, 1999; Philipp, 2012) either via a single open fracture or via a fracture network); ii) model-2, the "mobile hydrofracture" concept, suggests movement of thousands of isolated fluid batches through the crust and their accumulation in a structural trap near the final site of vein formation (e.g. Bons, 2001). Instant connection between the fluid reservoir and the final vein via a permanently open fracture therefore does not exist in this case.

In a fracture propagating from a source at depth ($h$) below the reference level (the studied deposit), the fluid overpressure ($P_o$) depends on the excess pressure ($P_e$) in the fluid source region, the fluid buoyancy effect (due to the density difference between the fluid in the fracture and the density of the rocks through which the fracture propagates) and the differential stress ($\sigma_D$) in the host rock (Gudmundsson, 1999):

$$P_o = P_e + (\rho_r - \rho_f)gh + \sigma_D \quad (13)$$

where $\rho_r$ is the density of the host rock, $\rho_f$ is the density of the fluid and $g$ is the acceleration due to gravity. During fracture formation, $P_e$ is equal to the tensile strength of the host rock of the fluid reservoir ($T_o = 6$ to 10 MPa is suggested as reliable estimate and $T_o = 15$ as the maximum value). The value of the differential stress is usually estimated from the general failure condition for the extensional veins ($\sigma_D = 4T_o$); however, an empirical linear relationships between $\sigma_D$ and $P_0$ as defined above is used. The equation above (Eq. (13)) can be rewritten so that the depth of the fluid source can be estimated:

$$h = \frac{P_o - (P_e + \sigma_D)}{(\rho_r - \rho_f)g} \quad (14)$$

Quartz veins ($Q_{1-2}$, $Q_2$ and possibly $Q_3$) at the Mokrsko-West deposit were formed from aqueous–carbonic fluids, with fluid densities varying from ca 750 to 850 kg m$^{-3}$; however, single values of $\rho_f = 770$ kg m$^{-3}$ and $\rho_r = 2650$ kg m$^{-3}$ are used in all the calculations. Partial separation of gasses (mainly $CO_2$) from the originally homogenous fluid phase could cause the variation of fluid density, but this is not encompassed in the model.

The depth of the hypothetical fluid source region for the Mokrsko deposit (Fig. 26) is based on the assumption that $P_e = 10$ MPa and on the above-established semi-empirical linear relationship between $P_o$ and $\sigma_D$ (Eq. (10)). Higher or lower values of $P_e$ (±5 MPa) have only a moderate effect on the estimated depth (±270 m). The squares mark the depth of the fluid source, suggesting a tensile strength of the Mokrsko tonalite equal to 5.5 MPa, while the diamonds correspond to $T_o = 15$ MPa. The minimum depth of the fluid source reservoir (model I) can be estimated at ca. 1 and 2 km below the level of the Mokrsko adit, or at 2 to 4 km, if higher tensile strength for the reservoir-host rocks is assumed ($T_o = 15$ MPa).

In general, the model suggests a much shallower depth of the fluid reservoir for the $Q_0$ veins than for the $Q_{1-2}$ and $Q_2$ veins. This is in agreement with an idea of a mostly local-(contact)-metamorphic source of the fluids responsible for the $Q_0$ veins and a deeper fluid source for the ore-bearing fluids. Finally, the model opens the hypothetical possibility of gradually increasing depth of the fluid reservoirs for the $Q_1$ through the $Q_2$ veins.

Simple geometrical analysis, based on the opposite sense of the dip of $J_1$ and $Q_{1-2}$ fractures at the Mokrsko-West and the Čelina deposits, points to their "intersection" at a depth of about 2.5 to 3.5 km below the adit level. This is compatible with the above calculations. A "fan" of parallel $J_1$ joints that tapped a single common fluid source region, however, should have produced a more or less homogeneously-distributed fan of quartz veins, which has not been found. The three deposits are separated by about 400–600 m wide zones that are almost devoid of quartz veins. Therefore, the existence of several disconnected fluid source regions and/or migration of the fluid source or of the fluid ascending paths in space and time is more probable.

### 5.4. Implications for the geological model of the Mokrsko deposit formation

Gold deposits and uneconomic gold prospects in the vicinity of CBPC are located preferentially along its NW-margin (e.g. Petráčkova hora, Jílové, Mokrsko deps.; Zachariáš et al., 2014, 2013, 2001), while they are almost absent inside the CBPC and much less frequent and of low economic importance along the SE-margin. Spatial distribution of the gold deposits thus seems to be controlled by an asymmetric thermal gradient across the volcano-plutonic arc.

The regional thermal gradient was first driven by the presence of the relatively cold Teplá-Barrandian Block to the NW and the relatively hot Moldanubian Block to the SE, while later the thermal effect of the CBPC predominated. The intrusion activity within the CBPC migrated through space and time: from the NE (~354 Ma; Sázava suite) to the SW (~345–347 Ma; Blatná suite). Later, numerous dikes and dike swarms of granite/granodiorite porphyries (most of them genetically related to the Blatná suite) intruded into almost whole area of the CPBC but are more frequent along the NW-margin. A period of ultrapotassic activity (~340–335 Ma), spatially concentrated in the middle of the SE-margin of the CBPC, postdates subsolidus deformation of the Blatná suite coupled with the down-dip of the Teplá-Barrandian and CBPC block. These ultrapotassic intrusions were followed by dike swarms of

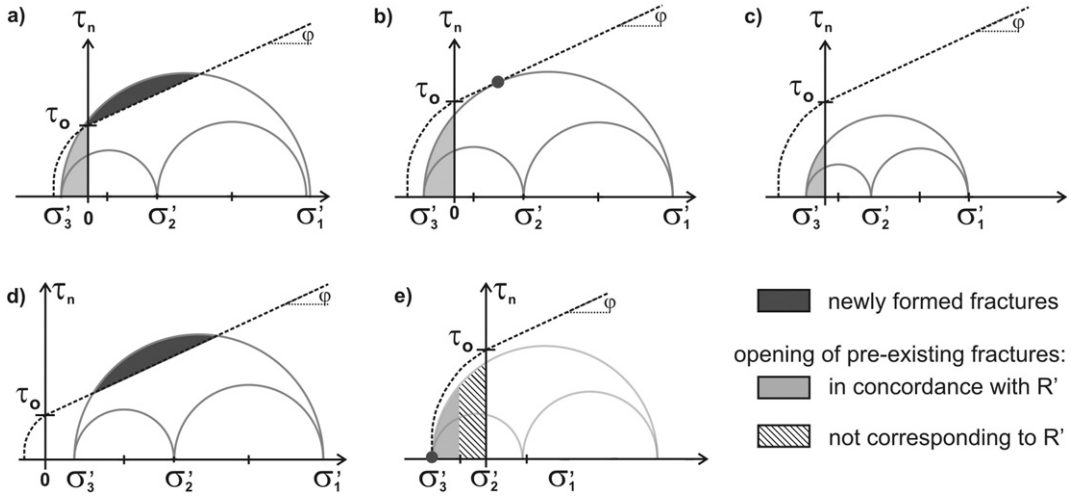


**Fig. 23.** Various hypothetical scenarios of formation of $Q_2$ extension veins by reopening of $J_1$ joints due to fluid overpressure and of formation of $Q_3$ shear veins by fracturing of "intact" rock. See the text for more details.

lamprophyres that are disseminated over whole area of the CBPC (and notably at the NW-margin).

Despite lateral migration of the main magmatic centers within the CBPC through space and time, the dike swarms associated with individual magmatic suites intruded almost the whole extent of the CBPC. The age difference between the dikes and their host-intrusions ranges from ~0 Ma up to 10–15 Ma. The much higher frequency of dikes near the NW-margin of the CBPC than in other parts may be interpreted as reflecting faster cooling below the ca 400–350 °C isotherm, making them prone to brittle fracturing. The same holds for the joints, fractures and minerals-filled fractures (i.e. veins). Similarly, we may expect that deep fluids irrespective of their origin (magmatic/metamorphic) tended to migrate in parallel with the decreasing thermal gradient, rather than in the opposite direction. This all explains the focusing of the ~347–339 Ma gold-bearing fluids predominantly along the NW-margin of the CBPC on a 100 km scale.

On a district scale, most gold-bearing quartz veins trend ~NW–SE or ~E–W (except for the Jílové gold district, where the main veins trend NNE–SSW; (Morávek, 1971; Zachariáš et al., 2013). This documents long-term NE–SW to N–S oriented horizontal extension above the subducted Saxothuringian plate, more or less parallel to the strike of the volcano-plutonic arc (the CBPC). This is in contrast with many subduction settings worldwide, where the extension in the overriding plate is usually parallel with the motion vector of the subducted plate (e.g. Sibson, 2013).

Quartz veins at the Mokrsko area form a network of interconnected steep veins (at least within the Mokrsko tonalite) that resemble the extension-fracture mesh abutting plutonic contacts (e.g. Cornubian batholith in SW England; Jackson et al., 1989), pointing to a lateral hydraulic gradient and fluids possibly dominated by magmatic component. An age difference of ca 10–12 Ma between the Mokrsko mineralization and its host-intrusion, however, excludes such simple analogy. This is further supported by ~2–4 km depth of the fluid source reservoir that supplied the fluid for the ore zone, as indicated by this study.

Numerous dikes that intruded the CBPC during the mid and late stages of its magmatic evolution could serve as loci of mechanical instability that facilitated up-flow of hydrothermal fluids (magmatic/metamorphic) to higher structural positions. Unambiguous examples of this fluid focusing are, however, restricted to only shallow settings (e.g. ~2–3 km), where they are represented by intense fracturing and hydrothermal alteration of the host dike (e.g. the Krásná Hora Sb-Au deposit; Němec and Zachariáš, 2015 and the Bohuliby mine of the Jílové Au deposit; Morávek, 1971; Zachariáš et al., 2013). Gold deposits formed at deeper crustal levels (e.g. 5–8 km; the Mokrsko and Petráčkova hora deposits), although dikes are also present, typically lack evidence for fluid focusing by these dikes (e.g. there is no correlation between the occurrence of the dikes and the frequency of veins; no alteration of the dikes is present and there are no fault zones hosting fracture-vein-mesh). Surprisingly, there is also no example of fluid focusing parallel to the intrusive/tectonic contacts of the CBPC (most contacts trend ~ NNE–SSW), either on a regional or on a local scale. This documents that the regional tectonic stress field was another main factor, in addition to the heat gradient, that caused the hydrothermal flow-lines to be more or less perpendicular to the strike of the volcano-plutonic-arc. A regional network of systematic parallel extension fractures ($J_1$ joints) oriented perpendicularly to the arc developed thus already in the early-cooling history of the pluton.

As mentioned above, an almost universal feature of gold-districts in the vicinity of the CBPC is their spatial proximity to intrusions of the CBPC and the overall coincidence of magmatic and hydrothermal processes on a regional scale. On deposit scales, the ore-forming processes are about 5–10 Ma younger than the magmatic-crystallization ages of their host intrusions (or spatially related intrusions). The difference is ~15 Ma at the Jílové deposit (Zachariáš et al., 2013), ~11.2 Ma at the Mokrsko-East deposit (Zachariáš and Stein, 2001) and ~3–4 Ma at the

**Table 3**
Estimation of the maximum magnitudes of the principal stresses necessary for reopening of the extensional $J_1$ joints and formation of the individual types of quartz veins at the Mokrsko-West deposit ($Q^E_{12}$ referrers to the Mokrsko-East deposit data set). Note the gradually decreasing values of the fluid overpressure ($P_o$) during $Q_0$ through $Q_2$ vein formation. Two alternative subsets of results are presented: the first subset is based on cohesion $\tau_o = 11$ MPa (based on the empirical failure envelope of (Hoek and Brown 1980) for the "very good quality granite"), while the second subset is based on cohesion $\tau_o = 30$ MPa (a common upper range for most igneous rocks). All the results are based on assumption of a fluid pressure ($P_f$) equal to 200 MPa and on the relation $\tau_o = 2T_o$ between the cohesion ($\tau_o$) and tensile strength ($T_o$).

| Vein type | Φ | $P_f$ (MPa) | $P_o$ (MPa) | $\tau_o$ (MPa) | $\sigma_D$ (MPa) | $\sigma_1$ (MPa) | $\sigma_2$ (MPa) | $\sigma_3$ (MPa) | $T_o$ (MPa) |
|---|---|---|---|---|---|---|---|---|---|
| $Q_0$ | 0.579 | 200 | 9.78 | 11.0 | 20.5 | 210.7 | 202.1 | 190.2 | 5.5 |
| $Q_1$ | 0.872 | 200 | 8.79 | 11.0 | 21.8 | 213.0 | 210.2 | 191.2 | 5.5 |
| $Q_{12}$ | 0.497 | 200 | 7.23 | 11.0 | 24.0 | 216.7 | 204.7 | 192.8 | 5.5 |
| $Q^E_{12}$ | 0.763 | 200 | 5.88 | 11.0 | 25.8 | 219.9 | 213.8 | 194.1 | 5.5 |
| $Q_2$ | 0.554 | 200 | 3.82 | 11.0 | 28.6 | 224.8 | 212.0 | 196.2 | 5.5 |
| $Q_0$ | 0.579 | 200 | 26.68 | 30.0 | 55.8 | 229.1 | 205.6 | 173.3 | 15.0 |
| $Q_1$ | 0.872 | 200 | 23.98 | 30.0 | 59.5 | 235.5 | 227.9 | 176.0 | 15.0 |
| $Q_{12}$ | 0.497 | 200 | 19.72 | 30.0 | 65.3 | 245.6 | 212.7 | 180.3 | 15.0 |
| $Q^E_{12}$ | 0.763 | 200 | 16.03 | 30.0 | 70.4 | 254.4 | 237.7 | 184.0 | 15.0 |
| $Q_2$ | 0.554 | 200 | 10.42 | 30.0 | 78.1 | 267.7 | 232.8 | 189.6 | 15.0 |

isolated Padrt' intrusion (Žák et al., 2014). A similar discrepancy between the crystallization age of the host-intrusion and the Re–Os age of hydrothermal molybdenite was encountered, for example, at the tungsten-bearing skarn of the Mactung deposit (Selby et al., 2003).

We can suggest that intrusion(s) genetically related to individual deposits are probably not exposed at the present erosional level. Numerous dike swarms spatially distributed over almost the whole extent of the CBPC clearly indicate active magmatic chamber(s) beneath the older already solidified intrusions. Geochemical data (fluid inclusions, stable isotopes, mineral chemistry) usually do not provide unambiguous evidence for solely magmatic (or magmatic-dominated) fluids responsible for the formation of gold-bearing quartz veins. Taking into account the spatial distribution of the gold deposits and the age-dissimilarity of the host intrusions and ores, two hypotheses are possible:

1) The gold deposits formed from hydrothermal fluids of deep-seated magmatic origin that exsolved from intrusions whose ascent stopped below the roof created by older and already solid intrusions. The magmatic fluids could mix on their ascent with external metamorphic fluids, a probable cause of their unequivocal geochemical characteristics. In its mechanical aspects, this model is analogous to the formation of swarms of late magmatic dikes.

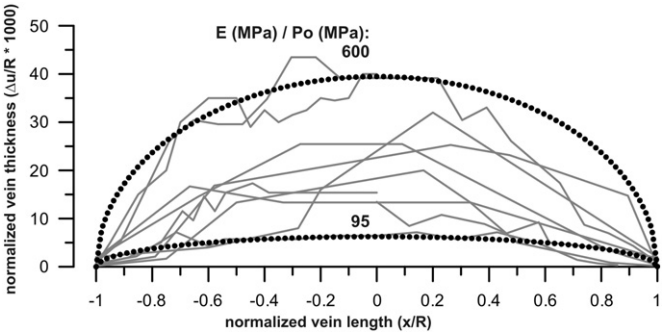


**Fig. 25.** Variations in the normalized quartz vein thickness (aperture) along the normalized vein length (distance). The thick dotted lines show the theoretical correlation between the vein thickness along the vein length, depending on the ratio of the Young's module (E), and the fluid overpressure ($P_o$). The theoretical lines are based on the Linear Elastic Fracture Model and constant fluid overpressure along whole vein length. All veins come from the Čelina-West deposit.

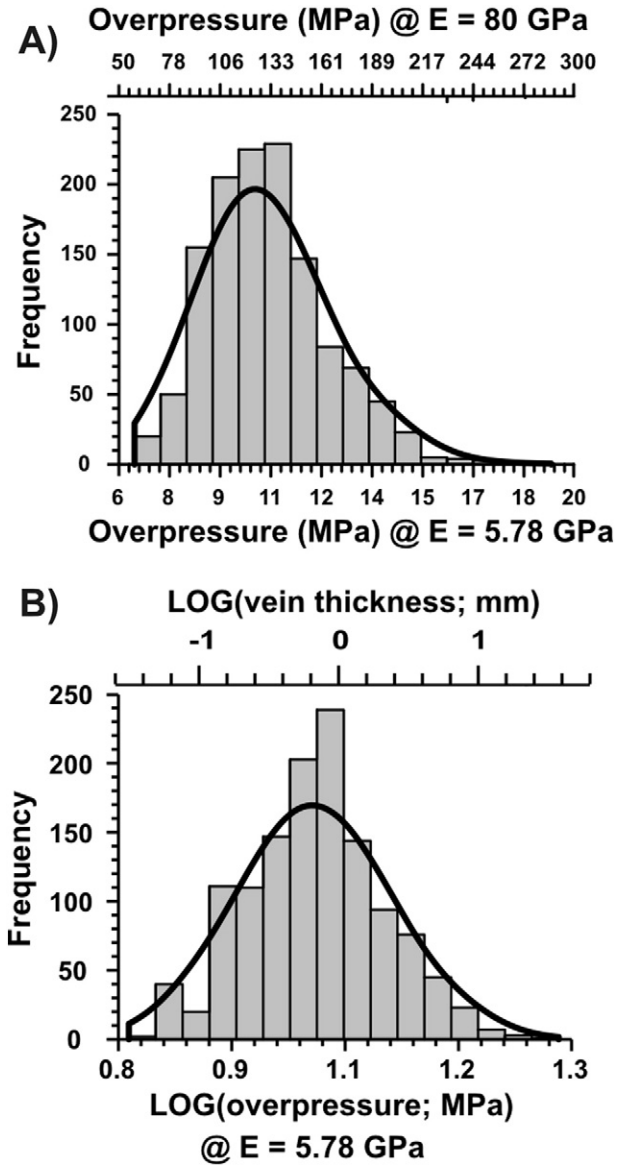


**Fig. 24.** Probable distribution of the fluid overpressure related to the formation of thin $Q_2$ veins in the Mokrsko tonalite, based on the hypothetical range of Young's module (E = 80 and 5.78 MPa) and a power–law relationship between the vein thickness and the vein aspect ratio.

2) The lower parts of the early intrusive phases acted as an irregular roof that could act as "lithological or structural traps" for deep-seated fluids (both of magmatic or metamorphic origins) along the more effectively cooled SW-margin of the CBPC. The traps either only delayed the fluids in their ascent or "locked" them until the traps were later tapped by brittle fractures (joint systems, faults and/or dikes) and the fluids were expelled due to their overpressure to higher structural positions and finally to the individual deposits. The spatial extent and timing of these processes were controlled by cooling of the rocks below the temperature of plastic deformation (~350–400 °C) and by local and regional tectonic stresses. Various numerical models (e.g. Žák et al., 2012) document that the granitic pluton can be effectively cooled down to less than 300 °C in 1–2 Ma, depending on a great many factors. Younger intrusions invading the older ones would, of course, retard the cooling rate, depending on their size. All this is in accordance with the observed gaps of about 15–2 Ma between the formation of the gold-bearing vein systems and the crystallization ages of their host or spatially-associated intrusions.

## 6. Conclusions

1) Detailed analysis of the structural data on both the deposit and regional scales allowed establishment of a general scenario of paleostress evolution and correlating it with the available geochronological data. Several switches between compression to transpression and extension regimes occurred during a ca 354–335 Ma period; the most common configuration was that with a subvertical intermediate principal stress axis.
2) Five generations of quartz veins (quartz gangue), referred to as $Q_0$ through $Q_4$, were distinguished, of which only the $Q_1$ through $Q_2$ veins are gold-bearing. However, it is possible to unambiguously distinguish between the $Q_1$ and $Q_2$ veins only within the tonalite of the Mokrsko-West deposit, where the two types differ markedly in thickness and spacing. Most of the veins at the Mokrsko-East and Čelina deposits are therefore referred to as being of the $Q_{1-2}$ type.
3) Formation of the $Q_{1-2}$ veins at the Mokrsko-East deposit was constrained to 342.9 ± 1.4 Ma by the Re–Os dating of molybdenite (Zachariáš and Stein, 2001).
4) Formation of the most frequent veins ($Q_1$, $Q_{1-2}$, $Q_2$) was associated with fluid-driven reopening of pre-existing extensional joints ($J_1$) caused by fluid overpressure. Two independent theoretical approaches were used to estimate the overpressure values that decrease from the $Q_0$ through the $Q_2$ veins. The absolute magnitudes of the principal stresses during vein formation ($Q_{1-2}$, $Q_2$) were

estimated by the combination of fluid inclusion data, Mohr-circle construction and the mechanical properties of the host rocks.

5) Most of the $Q_1$ and $Q_2$ veins also differ in the mechanism of their formation. For the $Q_1$ veins, multiple opening of the same fracture is common, pointing to the crack-seal mechanism of Ramsay (1980). Individual $Q_1$-gangue increments are, however, thicker (≥1 mm) than is common for classical crack-seal textures (~10–20 μm). Later deformation of the quartz gangue on a microscopic scale, coupled with a phase of regional brittle deformation, however, modified the original textures of most $Q_1$ and $Q_{1-2}$ veins. On the contrary, single-stage opening and filling is common for the $Q_2$ veins. This, together with the high frequency of $Q_2$ veins, indicates that a crack-jump mechanism as defined by Caputo and Hancock (1998) is the appropriate formation analog. Both mechanisms suggest different mechanical properties of the host rock and the gangue at the time of fracturing. The crack-seal mechanism implies that the tensile strength of the host rock is higher than that of the gangue, while the reverse is true for the crack-jump mechanism. The presence of both textures/mechanisms within a single-rock mass suggest a switch between these two mechanism during the relatively short period of the deposit evolution.
6) Spatially and host rock-related trends were demonstrated for the vein thickness and spacing. Both parameters increase from the interior of the tonalite towards its contact and further away from the contact, when the veins are hosted by the Jílové Belt rocks.
7) The $Q_{1-2}$ veins have the form of a horizontally elongated ellipse, whose mean axes ratio varies from 222:139:1 to 169:124:1 for the 10 and 600 mm thick veins, respectively. The vein aspect ratio (mean trend) seems to be more or less constant and independent of the vein thickness for the early veins ($Q_1$ and $Q_{1-2}$), while it appears to correlate inversely with the thickness of the thin $Q_2$ veins. This suggests that the fluid overpressure was more or less constant during the formation of the early veins, but decreased gradually or oscillated during the formation of the thin $Q_2$ veins.
8) Based on the principles of linear elastic fracture mechanics, the probable depth of the fluid source reservoir(s) for the $Q_2$ veins was estimated at ~2 to ~4 km below the present surface. Fluid source depth might evolve through time, being the shallowest for the $Q_0$ veins and the deepest for the $Q_2$ veins.
9) Two hypothetical models of fluid-source-reservoir occurrence/trapping below the solidified roof of the early and mid-stage intrusions of the Central Bohemian Plutonic Complex (CBPC) are described, in order to explain the marked spatial distribution of most gold districts/deposits at/near contacts with the granitic rocks of the CBPC and the systematic difference of about 15–2 Ma between the formation of the gold-bearing vein systems (inferred from Re–Os molybdenite age-data) and the crystallization-ages of their host- or spatially-associated intrusions.

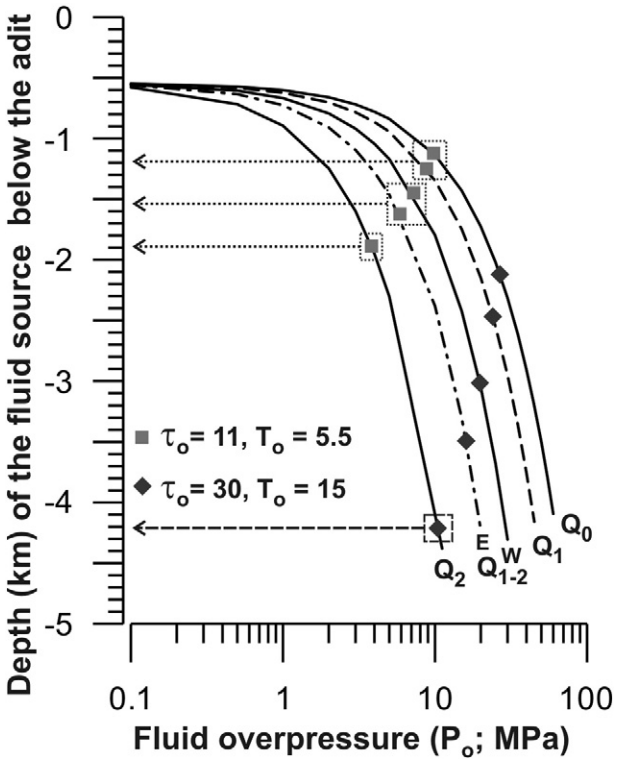


**Fig. 26.** Estimation of the probable depth of the fluid source reservoir of individual types of quartz veins in the Mokrsko district. The model is based on the dependence of the fluid overpressure during the vein formation on the differential stress, the tensile strength and the elastic properties of the fracture–host and reservoir–host rocks. Two alternative scenarios are presented. The first one (squares) suggests lower tensile strength for the Mokrsko tonalite than the second one (diamonds). See the text for a more detailed discussion.

## Acknowledgments

Preparation of the manuscript benefited from the support of the Ministry of Education of the Czech Republic to the Faculty of Science of Charles University (project PRVOUK P44) and from a project OPPK CZ.2.16/3.1.00/21516. Madeleine Štulíková is thanked for revision of the English language. Peter Morávek is thanked for providing the access to documents from the period of exploration. Detailed reviews of T. Blenkinsop and another anonymous reviewer are also greatly acknowledged, as well as the editorial comments of H. G. Dill.

## References

André, A.-S., Sausse, J., Lespinasse, M., 2001. New approach for the quantification of paleostress magnitudes: application to the Soultz vein system (Rhine graben, France). Tectonophysics 336, 215–231.
Baker, T., 2002. Emplacement depth and carbon dioxide-rich fluid inclusions in intrusion-related gold deposits. Econ. Geol. 97, 1111–1117.
Boiron, M.C., Barakat, A., Cathelineau, M., Banks, D.A., Durisová, J., Morávek, P., 2001. Geometry and P–V–T–X conditions of microfissural ore fluid migration: the Mokrsko gold deposit (Bohemia). Chem. Geol. 173, 207–225.
Bons, P.D., 2001. The formation of large quartz veins by rapid ascent of fluids in mobile hydrofractures. Tectonophysics 336, 1–17.
Brooks Clark, M., Brantley, S.L., Fisher, D.M., 1995. Power-law vein-thickness distributions and positive feedback in vein growth. Geology 23, 975–978.
Caputo, R., Hancock, P.L., 1998. Crack-jump mechanism and its implications for stress cyclicity during extension fracturing. J. Geodyn. 27, 45–60.
Cervantes, P., Wiltschko, D.V., 2010. Tip to midpoint observations on syntectonic veins, Ouachita orogen, Arkansas: trading space for time. J. Struct. Geol. 32, 1085–1100.
Duuring, P., Cassidy, K.F., Hagemann, S.G., 2007. Granitoid-associated orogenic, intrusion-related, and porphyry style metal deposits in the Archean Yilgarn Craton, Western Australia. Ore Geol. Rev. 32, 157–186.
Faryad, S.W., Kachlík, V., Sláma, J., Hoinkes, G., 2015. Implication of corona formation in a metatroctolite to the granulite facies overprint of HP–UHP rocks in the Moldanubian Zone (Bohemian Massif). J. Metamorph. Geol. 33, 295–310.
Fediuk, F., 1992. Metaboninite in the Proterozoic Jílové Belt of Central Bohemia. Věst. Ústř. Úst. Geol. 67, 297–310 (Prague).
Fediuk, F., 2004. Alaskites and related rocks in the Proterozoic Jílové Belt of central Bohemia. Krystalinikum 30, 27–50.
Foxford, K.A., Nicholson, R., Polya, D.A., Hebblethwaite, R.P.B., 2000. Extensional failure and hydraulic valving at Minas da Panasqueira, Portugal: evidence from vein spatial distributions, displacements and geometries. J. Struct. Geol. 22, 1065–1086.
Gudmundsson, A., 1999. Fluid overpressure and stress drop in fault zones. Geophys. Res. Lett. 26, 115–118. http://dx.doi.org/10.1029/1998GL900228.
Gudmundsson, A., 2000. Fracture dimensions, displacements and fluid transport. J. Struct. Geol. 22, 1221–1231.
Gudmundsson, A., 2004. Effects of Young's modulus on fault displacement. Compt. Rendus Geosci. 336, 85–92.
Gudmundsson, A., 2011. Rock Fractures in Geological Processes. Cambridge University Press, Cambridge (578 pp.).
Gudmundsson, A., Kusumoto, S., Simmenes, T.H., Philipp, S.L., Larsen, B., Lotveit, I.F., 2012. Effects of overpressure variations on fracture apertures and fluid transport. Tectonophysics 581, 220–230.
Gumiel, P., Martín-Izard, A., Arias, M., Rodríguez-Terente, L., 2008. Geometrical analysis of the Punta del Pedrón shear zone (Asturias, Spain): implications related to exploration of Salave Gold-type mineralization. J. Struct. Geol. 30, 354–365.

Guy, A., Edel, J.B., Schulmann, K., Tomek, C., Lexa, O., 2011. A geophysical model of the Variscan orogenic root (Bohemian Massif): implications for modern collisional orogens. Lithos 124, 144–157.
Hajná, J., Žák, J., Kachlík, V., 2011. Structure and stratigraphy of the Teplá-Barrandian Neoproterozoic, Bohemian Massif: a new plate-tectonic reinterpretation. Gondwana Res. 19, 495–508.
Havlíček, V., 1981. Development of a linear sedimentary depression exemplified by the Prague Basin (Ordovician: middle Devonian; Barrandian area, Central Bohemia). Sb. Geol. Věd (Geol.) 35, 7–48.
Hoek, E., Brown, E.T., 1980. Empirical strength criterion for rock masses. J. Geotech. Eng. Div. 106 (GT9), 1013–1035.
Hoek, E., Brown, E., 1988. The Hoek-Brown failure criterion — a 1988 update. In: Curran, J. (Ed.), Proc. 15th Canadian Rock Mech. Symp. Civil Engineering Dept., University of Toronto, Toronto.
Holland, M., Urai, J.L., 2010. Evolution of anastomosing crack-seal vein networks in limestones: Insight from an exhumed high-pressure cell, Jabal Shams, Oman Mountains. J. Struct. Geol. 32, 1279–1290.
Holub, F.V., Cocherie, A., Rossi, P., 1997b. Radiometric dating of granitic rocks from the Central Bohemian Plutonic Complex (Czech Republic): constraints on the chronology of thermal and tectonic events along the Moldanubian–Barrandian boundary. Compt. Rendus Geosci. 325, 19–26.
Holub, F., Machart, J., Manová, M., 1997a. The Central Bohemian plutonic Complex Geology, chemical composition and genetic interpretation. Sb. Geol. Věd, Lož. Geol. Miner. 31, 27–50 (Prague).
Jackson, N.J., Willis-Richards, J., Manning, D.A.C., Sams, M.S., 1989. Evolution of the Cornubian ore field, southwest England: part II. Mineral deposits and ore-forming processes. Econ. Geol. 84, 1101–1133.
Janoušek, V., Gerdes, A., 2003. Timing the magmatic activity within the Central Bohemian Pluton, Czech Republic: conventional U–Pb ages for the Sázava and Tábor intrusions and their geotectonic significance. J. Czech Geol. Soc. 48, 70–71 (Prague).
Janoušek, V., Braithwaite, C.J.R., Bowes, D.R., Gerdes, A., 2004. Magma-mixing in the genesis of Hercynian calc-alkaline granitoids: an integrated petrographic and geochemical study of the Sazava intrusion, Central Bohemian Pluton, Czech Republic. Lithos 78, 67–99.
Janoušek, V., Wiegand, B.A., Žák, J., 2010. Dating the onset of Variscan crustal exhumation in the core of the Bohemian Massif: new U–Pb single zircon ages from the high-K calc-alkaline granodiorites of the Blatna suite, Central Bohemian Plutonic Complex. J. Geol. Soc. Lond.
Johnston, J.D., McCaffrey, K.J.W., 1996. Fractal geometries of vein systems and the variation of scalingrelationships with mechanism. J. Struct. Geol. 18, 349–358.
Jolly, R.J.H., Sanderson, D.J., 1997. A Mohr circle construction for the opening of a pre-existing fracture. J. Struct. Geol. 19, 887–892.
Kontak, D.J., Kyser, K., 2011. A fluid inclusion and isotopic study of an intrusion-related gold deposit (IRGD) setting in the 380 Ma South Mountain Batholith, Nova Scotia, Canada: evidence for multiple fluid reservoirs. Mineral. Deposita 46, 337–363.
Ladeira, F., Price, N., 1981. Relationship between fracture spacing and bed thickness. J. Struct. Geol. 3, 179–183.
Linnemann, U., Pereira, F., Jeffries, T.E., Drost, K., Gerdes, A., 2008. The Cadomian orogeny and the opening of the Rheic Ocean: the diacrony of geotectonic processes constrained by LA-ICP-MS U–Pb zircon dating (Ossa-Morena and Saxo-Thuringian Zones, Iberian and Bohemian Massifs). Tectonophysics 461, 21–43.
Mandl, G., 2005. Rock Joints. The Mechanical Genesis. 1st ed. Springer-Verlag, Berlin (221 pp.).
Morávek, P., 1971. Ore-deposits structure and mineralization of the Jílové gold-mining district. Sb. Geol. Věd. Lož. Geol. 13, 1–170 (Prague).
Morávek, P., 1996a. Gold deposits of the Central and SW part of the Bohemian Massif. In: Morávek, P. (Ed.), Gold Deposits in Bohemia. Czech Geological Survey, Prague, pp. 1–16.
Morávek, P., 1996b. The Mokrsko gold deposit. In: Morávek, P. (Ed.), Gold Deposits in Bohemia. Czech Geological Survey, Prague, pp. 31–56.
Morávek, P., Fediuk, F., Röhlich, P., Váňa, T., 1994. Geological map of the Jílové Belt 1: 25 000 and Explanations.
Morávek, P., Litochleb, J., Sejkora, J., Škoda, R., 2010. Pegmatity s molybdenitem u Skalska na Jílovsku, Česká republika - historie, geologie a mineralogie (The pegmatites with molybdenite near Skalsko on the Jílové area, Czech Republic — history, geology and mineralogy). Bull. Miner. Odd. Nár. Muz. 18, 1–21.
Morávek, P., Röhlich, P., Váňa, T., Fatková, J., Fediuk, F., Janatka, J., Waldhausrová, J., Pacáková, L., Fuksa, J., Morch, M., Jilemnický, Z., 1991a. The Jílové Belt — Final Report. Geoindustria, Prague Unpublished report.
Morávek, P., Straka, E., Hron, M., Janatka, J., Šouta, M., Štěpař, B., Svoboda, K., Rössler, J., Cihelka, J.V.H., Unzeitig, M., Koroš, I., Hercík, M., Fatková, J., Malec, J., Pertoldová, J., Straková, S., Kavalec, J., Soukup, B., Buriánová, D., Bubeníček, J., Neumannová, Š., 1990. Mokrsko-West — Final Report and Resources Evaluation. Geoindustria, Prague Unpublished report.
Morávek, P., Straka, E., Seidl, K., Fatková, J., Janatka, J., Koroš, I., Hron, M., Kavalec, J., Brtna, M., Rössler, J., 1991b. Čelina — Psí Hory — Final Report and Resources Evaluation. Geoindustria, Prague Unpublished report.
Němec, M., Zachariáš, J., 2015. The Krásná Hora epizonal orogenic Sb–Au deposit, Bohemian Massif, Czech Republic. In: André-Mayer, A.S., Cathelineau, M., Muchez, P., Pirard, E., Sindern, S. (Eds.), Mineral Resources in a Sustainable World. Proceeding of the 13th Biennial SGA Meeting, 24–27 August 2015, Nancy, France, pp. 497–500.
Olson, J.E., Schultz, R.A., 2011. Comment on "A note on the scaling relations for opening mode fractures in rock" by C.H. Scholz. J. Struct. Geol. 33, 1523–1524.
Otto, B.R., Piekenbrock, J., Odden, J., 2009. Structural evolution of the rock creek gold deposit, Seward Peninsula, Alaska. Econ. Geol. 104, 945–960.
Penczak, R.S., Mason, R., 1997. Metamorphosed archean epithermal Au–As–Sb–Zn–(Hg) vein mineralization at the Campbell Mine, Northwestern Ontario. Econ. Geol. 92, 696–719.
Philipp, S.L., 2012. Fluid overpressure estimates from the aspect ratios of mineral veins. Tectonophysics 581, 35–47.
Pitra, P., Burg, J., Guiraud, M., 1999. Late Variscan strike-slip tectonics between the Tepla-Barrandian and Moldanubian terranes (Czech Bohemian Massif): petrostructural evidence. J. Geol. Soc. Lond. 156, 1003–1020.
Pollard, D.D., Segall, P., 1987. Theoretical displacements and stresses near fractures in rock: with applications to faults, joints, veins, dikes, and solution surfaces. Fracture Mechanics of Rock. Academic Press Inc. Ltd., London, pp. 277–349.
Rajlich, P., 1988. Tectonics of the NW border of the Central Bohemian Pluton and the Variscan transpression of the Bohemicum block structure. J. Geol. Sci. Geol. PragueSciences, Geol. 43, pp. 9–72
Rajlich, P., 1993. Variscan Ductile Tectonics of the Bohemian Massif. Czech Geological Survey, Prague (172 pp., (in Czech)).
Rajlich, P., Schulmann, K., Synek, J., 1988. Strain analysis of conglomerates in the Central Bohemian shear zone. Krystalinikum 19, 119–134.
Ramsay, J.G., 1980. The crack-seal mechanism of rock deformation. Nature 284, 135–139.
Sanderson, D.J., Roberts, S., Gumiel, P., Greenfield, C., 2008. Quantitative analysis of tin- and tungsten-bearing sheeted vein systems. Econ. Geol. 103, 1043–1056.
Scholz, C.H., 2010. A note on the scaling relations for opening mode fractures in rock. J. Struct. Geol. 32, 1485–1487.
Schulmann, K., Konopásek, J., Janoušek, V., Lexa, O., Lardeaux, J.M., Edel, J.B., Štípská, P., Ulrich, S., 2009. An Andean type Palaeozoic convergence in the Bohemian Massif. Compt. Rendus Geosci. 341, 266–286.
Schulmann, K., Lexa, O., Janoušek, V., Lardeaux, J.M., Edel, J.B., 2014. Anatomy of a diffuse cryptic suture zone: an example from the Bohemian Massif, European variscides. Geology 42, 275–278.
Schultz, R.A., Klimczak, C., Fossen, H., Olson, J.E., Exner, U., Reeves, D.M., Soliva, R., 2013. Statistical tests of scaling relationships for geologic structures. J. Struct. Geol. 48, 85–94.
Selby, D., Creaser, R.A., Heaman, L.M., Hart, C.J., 2003. Re–Os and U–Pb geochronology of the Clear Creek, Dublin Gulch, and Mactung deposits, Tombstone Gold Belt, Yukon, Canada: absolute timing relationships between plutonism and mineralization. Can. J. Earth Sci. 40, 1839–1852.
Sibson, R.H., 2007. An episode of fault-valve behaviour during compressional inversion? — the 2004 MJ6.8 Mid-Niigata Prefecture, Japan, earthquake sequence. Earth Planet. Sci. Lett. 257, 188–199.
Sibson, R.H., 2013. Stress switching in subduction forearcs: implications for overpressure containment and strength cycling on megathrusts. Tectonophysics 600, 142–152.
Sibson, R.H., Rowland, J.V., 2003. Stress, fluid pressure and structural permeability in seismogenic crust, North Island, New Zealand. Geophys. J. Int. 154, 584–594.
Simpson, G.D.H., 2000. Synmetamorphic vein spacing distributions: characterisation and origin of a distribution of veins from NW Sardinia, Italy. J. Struct. Geol. 22, 335–348.
Strnad, L., Goliáš, V., Mihaljevič, M., Pudilová, M., 2012. The Variscan Kašperské Hory orogenic gold deposit, Bohemian Massif, Czech Republic. Ore Geol. Rev. 48, 428–441.
Thompson, J.F.H., Sillitoe, R.H., Baker, T., Lang, J.R., Mortensen, J.K., 1999. Intrusion-related gold deposits associated with tungsten–tin provinces. Mineral. Deposita 34, 323–334.
Vermilye, J.M., Scholz, C.H., 1995. Relation between vein length and aperture. J. Struct. Geol. 17, 423–434.
Von Raumer, J.F., Stampfli, G.M., Borel, G., Bussy, F., 2002. Organization of pre-Variscan basement areas at the north-Gondwanan margin. Int. J. Earth Sci. 91, 35–52.
Waldhausrová, J., 1984. Proterozoic volcanites and intrusive rocks of the Jílové zone in Central Bohemia. Krystalinikum 17, 77–97.
Waldhausrová, J., 1997. Proterozoic volcanics geochemistry and mineral chemistry: a contribution to the Barrandian Upper Proterozoic stratigraphy (Bohemian Massif, Czech Republic). Krystalinikum 23, 151–180.
Zachariáš, J., Stein, H., 2001. Re–Os ages of Variscan hydrothermal gold mineralisations, Central Bohemian metallogenetic zone. In: Piestrzyński, et al. (Eds.), Mineral Deposits at the Beginning of the 21st Century. Swets & Zeitlinger Publishers, Lisse, pp. 851–854.
Zachariáš, J., Morávek, P., Gadas, P., Pertoldová, J., 2014. The Mokrsko-West gold deposit, Bohemian Massif, Czech Republic: mineralogy, deposit setting and classification. Ore Geol. Rev. 58, 238–263.
Zachariáš, J., Paterová, B., Pudilová, M., 2009. Mineralogy, fluid inclusion, and stable isotope constraints on the genesis of the Roudny Au–Ag deposit, Bohemian Massif. Econ. Geol. 104, 53–72.
Zachariáš, J., Pertold, Z., Pudilová, M., Žák, K., Pertoldová, J., Stein, H., Markey, R., 2001. Geology and genesis of Variscan porphyry-style gold mineralization, Petráčkova hora deposit, Bohemian Massif, Czech Republic. Mineral. Deposita 36, 517–541.
Zachariáš, J., Žák, K., Pudilová, M., Snee, L.W., 2013. Multiple fluid sources/pathways and severe thermal gradients during formation of the Jílové orogenic gold deposit, Bohemian Massif, Czech Republic. Ore Geol. Rev. 54, 81–109.
Žák, J., Holub, F.V., Verner, K., 2005a. Tectonic evolution of a continental magmatic arc from transpression in the upper crust to exhumation of mid-crustal orogenic root recorded by episodically emplaced plutons: the Central Bohemian Plutonic Complex (Bohemian Massif). Int. J. Earth Sci. 94, 385–400.
Žák, J., Schulmann, K., Hrouda, F., 2005b. Multiple magmatic fabrics in the Sázava pluton (Bohemian Massif, Czech Republic): a result of superposition of wrench-dominated regional transpression on final emplacement. J. Struct. Geol. 27, 805–822.
Žák, J., Dragoun, F., Verner, K., Chlupáčová, M., Holub, F.V., Kachlík, V., 2009. Forearc deformation and strain partitioning during growth of a continental magmatic arc: The northwestern margin of the Central Bohemian Plutonic Complex, Bohemian Massif. Tectonophysics 469, 93–111.

Žák, K., Svojtka, M., Breiter, K., Ackerman, L., Zachariáš, J., Pašava, J., Veselovský, F., Litochleb, J., Ďurišová, J., Haluzová, E., 2014. Padrť Stock (Teplá-Barrandian Unit, Bohemian Massif): petrology, geochemistry, U–Pb zircon dating of granodiorite, and Re–Os age and origin of related molybdenite mineralization. J. Geosci. 59, 351–366.

Žák, J., Verner, K., Holub, F.V., Kabele, P., Chlupáčová, M., Halodová, P., 2012. Magmatic to solid state fabrics in syntectonic granitoids recording early Carboniferous orogenic collapse in the Bohemian Massif. J. Struct. Geol. 36, 27–42.

Žalohar, J., Vrabec, M., 2007. Paleostress analysis of heterogeneous fault-slip data: The Gauss method. J. Struct. Geol. 29, 1798–1810.